RESEARCH ARTICLE

Isolation of bioactive compounds from the petroleum ether soluble fraction of *Eichhornia crassipes* (Mart.) Solms flowers with dual evaluation: *In silico* studies of isolated molecules and *in vitro*/*in vivo* activities of the extract

Md. Mirazul Islam[1☯*], **Suriya Akter Shompa**[1,2☯], **Hasin Hasnat**[1☯], **Safaet Alam**[2,3*], **Saima Jahan Riti**[1], **Ferdousy Kabir**[1], **Md. Sakhawat Hossain**[4], **Mohammad A. Rashid**[2]

1 Department of Pharmacy, School of Pharmaceutical Sciences, State University of Bangladesh, Dhaka, Bangladesh, **2** Department of Pharmaceutical Chemistry, Faculty of Pharmacy, University of Dhaka, Dhaka, Bangladesh, **3** Chemical Research Division, BCSIR Dhaka Laboratories, Bangladesh Council of Scientific and Industrial Research (BCSIR), Dhaka, Bangladesh, **4** Pharmaceutical Sciences Research Division, BCSIR Dhaka Laboratories, Bangladesh Council of Scientific and Industrial Research (BCSIR), Dhaka, Bangladesh

☯ These authors contributed equally to this work.
* mirazul.pharmacy@sub.edu.bd (MMI); safaet.du@gmail.com (SA)

Check for updates

OPEN ACCESS

Citation: Islam MM, Shompa SA, Hasnat H, Alam S, Riti SJ, Kabir F, et al. (2026) Isolation of bioactive compounds from the petroleum ether soluble fraction of *Eichhornia crassipes* (Mart.) Solms flowers with dual evaluation: *In silico* studies of isolated molecules and *in vitro*/*in vivo* activities of the extract. PLoS One 21(6): e0351085. https://doi.org/10.1371/journal.pone.0351085

Editor: Javed Iqbal, University of Sahiwal, PAKISTAN

Received: December 1, 2025

Accepted: May 19, 2026

Published: June 8, 2026

Copyright: © 2026 Islam et al. This is an open access article distributed under the terms of the Creative Commons Attribution License, which permits unrestricted use, distribution, and reproduction in any medium, provided the original author and source are credited.

Data availability statement: All relevant data are within the manuscript and its Supporting information files.

Abstract

Eichhornia crassipes (water hyacinth), an invasive aquatic plant, has attracted interest as a potential source of pharmacologically active natural products despite its ecological impact. The present study investigated the petroleum ether soluble fraction (PSF) of the methanolic extract of E. crassipes flowers to identify bioactive constituents and evaluate their biological activities. Chromatographic isolation followed by ^{1}H NMR spectroscopy led to the identification of five compounds: Kaempferol (Compound 1), Luteolin (Compound 2), Stigmasterol (Compound 3), 4-carboxybenzyl alcohol (Compound 4), and 4-methoxybenzaldehyde (Compound 5). Antimicrobial activity was assessed using disc diffusion and minimum inhibitory concentration (MIC) assays, thrombolytic activity through an in vitro clot lysis method, and antidiarrheal activity using the castor oil–induced diarrhea model in mice. Molecular docking and ADMET analyses were performed to explore potential target interactions and pharmacokinetic characteristics. The PSF exhibited moderate antimicrobial activity, with the highest inhibition against *Bacillus subtilis* (20.33 ± 1.25 mm) and MIC values ranging from 15.6–500 µL/mL. The extract also produced 14% clot lysis in the thrombolytic assay. *In vivo* antidiarrheal testing showed dose-dependent inhibition, reaching 38.89% reduction in diarrheal count at 600 mg/kg, approaching the activity of loperamide. Molecular docking analysis revealed that the identified compounds exhibited potential binding affinities comparable to standard ligands, suggesting potential interactions with relevant biological targets. The stigmasterol showing the highest interaction toward the κ-opioid receptor (−10.3 kcal/mol), comparable to

Funding: The author(s) received no specific funding for this work.

Competing interests: The authors have declared that no competing interests exist.

loperamide (−9.1 kcal/mol). Flavonoids such as kaempferol and luteolin demonstrated notable binding with antimicrobial targets including dihydrofolate reductase (DHFR) and β-ketoacyl-ACP synthase (KAS), as well as thrombolytic target tissue plasminogen activator (TPA). ADMET predictions indicated favorable drug-likeness for the flavonoids but highlighted lipophilicity-related limitations for stigmasterol. Collectively, these findings highlight the PSF of *E. crassipes* as a promising reservoir of multi-target phytochemicals with potential applications in gastrointestinal, infectious, and thromboembolic disorders.

Introduction

For centuries, plants have served as a fundamental source of therapeutic agents, playing a pivotal role in global healthcare [1]. The World Health Organization reports that nearly 80% of the world's population relies on traditional medicine, highlighting the continued relevance of plant-based treatments [2]. Compared to synthetic drugs, plant-derived medicines are often associated with therapeutic efficacy and reduced adverse effects, which supports their widespread use in traditional systems such as Ayurveda and Chinese medicine [3]. These systems utilize diverse bioactive compounds that continue to attract attention for the development of novel therapeutics [4]. Projections further suggest that plant-based therapies may constitute a substantial proportion of medicines, particularly in developing regions [5]. In the modern era, medicinal plants remain a promising source for managing conditions such as pain, oxidative stress, cancer, and other chronic diseases, owing to their accessibility, cost-effectiveness, and therapeutic potential [3].

Eichhornia crassipes, or water hyacinth, is an invasive aquatic plant native to South America's Amazon basin [6]. It has spread globally, adapting to various climates and aquatic environments, from lakes to rivers, disrupting ecological balance. The plant is characterized by its round to oval leaves, covered petioles, and blue or lavender flowers. Its air-filled sacs enable it to float on water, while its extensive root system facilitates nutrient absorption [6,7]. Despite its ecological impact, water hyacinth has been utilized in traditional medicine worldwide. In Chinese medicine, it is used to support spleen health, while in the Philippines, it serves as an anti-inflammatory agent. In Kenya, it aids lactation and menstrual regulation, and its beans are consumed to alleviate digestive issues. Modern research has identified its potential anti-cancer properties, alongside its antifungal, antibacterial, and wound-healing abilities [2,8].

Taxonomically, water hyacinth belongs to the Pontederiaceae family and is rich in bioactive compounds such as alkaloids, flavonoids, and terpenoids. These compounds contribute to its neuropharmacological effects, including analgesic, anti-epileptic, and memory-enhancing properties [2]. The plant also exhibits hepatoprotective, antioxidant, and antitumor activities, making it a valuable resource for pharmaceutical and cosmetic applications. Its ability to absorb heavy metals further

underscores its utility in phytoremediation. The diverse phytochemical composition of water hyacinth supports its use in treating gastrointestinal disorders, inflammation, and pain, highlighting its significance in both traditional and modern medicine [9,10].

Global health issues, including diarrheal diseases and the rise of antimicrobial resistance (AMR), highlight the critical need for innovative therapeutic solutions. Diarrheal diseases remain a major global health concern, contributing to approximately 1.5 million deaths annually worldwide, with recent estimates from the Global Burden of Disease (GBD 2021) study indicating that this burden remains substantial, particularly in low- and middle-income countries [11,12]. One of the main causes of diarrheal mortality is poor sanitation and infections caused by pathogens such as *Candida albicans, Escherichia coli*, and *Salmonella typhi* [13,14]. In addition, antimicrobial resistance represents a major global health threat, and projections suggest that AMR could cause up to 10 million deaths per year by 2050 if effective interventions are not implemented [15]. Although a wide range of synthetic drugs is available for treating infections, these often come with substantial side effects [2]. On the other hand, plant-based medicines are increasingly recognized for their enhanced therapeutic efficacy and reduced adverse effects [16]. Resulting increased interest in plant-based antimicrobial agents as potential alternatives to traditional antibiotics for tackling these pressing health concerns. Consequently, the development of new antibacterial agents derived from natural sources holds promise in controlling bacterial proliferation and addressing the issue of antimicrobial resistance [1]. Natural plant-based compounds have recently emerged as a valuable reservoir of novel, safe, and potent bioactive metabolites with significant therapeutic potential.

This study aimed to investigate the phytochemical composition and pharmacological potential of *Eichhornia crassipes* flower extracts through an integrated analytical and biological approach. Chromatographic separation combined with ^{1}H NMR spectroscopy was employed to identify the major phytochemical constituents present in the petroleum ether soluble fraction. The biological activities of the extract were subsequently evaluated using in vitro antimicrobial and thrombolytic assays, along with *in vivo* antidiarrheal experiments. To explore possible molecular mechanisms underlying these activities, molecular docking analysis was performed to predict potential interactions between the identified compounds and selected biological targets. This computational approach was used to generate hypothesis-supporting insights rather than definitive mechanistic conclusions. By integrating phytochemical characterization with experimental pharmacological evaluation and predictive *in silico* analysis, the study provides a comprehensive assessment of the bioactive potential of *E. crassipes* flowers, while highlighting the need for further mechanistic and pharmacological validation.

Materials and methods

Drugs and chemicals

High-purity analytical-grade drugs and chemicals were utilized in this study. Methanol, Petroleum Ether, Dichloromethane, Ethyl Acetate and Tween-80 were obtained from Merck (Darmstadt, Germany). Loperamide, Streptokinase, Azithromycin, Amoxicillin, Ciprofloxacin, and Fluconazole were procured from Square Pharmaceuticals Ltd. and Beximco Pharmaceuticals Ltd, both located in Bangladesh.

Microorganism

For the antimicrobial evaluation, a range of microorganisms was used, including gram-positive bacteria (*Sarcina lutea*, *Bacillus megaterium*, *Staphylococcus aureus*, *Bacillus cereus*, and *Bacillus subtilis*), gram-negative bacteria (*Vibrio mimicus*, *Pseudomonas aeruginosa*, *Salmonella typhi*, *Salmonella paratyphi*, *Escherichia coli*, *Shigella dysenteriae*, and *Vibrio parahaemolyticus*), and fungal strains (*Aspergillus niger*, *Saccharomyces cerevisiae*, and *Candida albicans*). These microbial strains were obtained from the University of Dhaka, Bangladesh.

Plant collection

On November 11, 2022, the flowers of *Eichhornia crassipes* (Mart.) Solms were gathered from the Hawor region of Austagram, Kishoreganj, Dhaka, Bangladesh. The plant specimen was verified by a botanist at the Bangladesh National Herbarium on December 6, 2022, and given the unique accession number DACB87254. The plant material was then processed and stored in the phytochemical laboratory of the School of Pharmacy at the State University of Bangladesh for experimental purposes.

Extraction process

The flower of *E. crassipes* was thoroughly cleaned and shed dried until the moisture content was reduced to around 10%. The dried plant was then ground into a coarse powder using a grinding machine. Approximately 800 grams of the powdered flowers were placed in a 5-liter round-bottomed flask, and 2.5 liters of methanol were added. The mixture was allowed to macerate for 21 days, with regular shaking and stirring. After maceration, the mixture (32% w/v) was filtered through Whatman No. 1 filter paper and a fresh cotton plug. This extraction process was repeated three times using analytical-grade ethanol. The combined filtrate was concentrated using a Buchi Rotavapor under reduced temperature and pressure, resulting in 83.5 grams of crude extract (10.43% yield).

To fractionate the crude extract, a modified Kupchan partitioning method was employed following established protocols [17]. Briefly, 50 g of the concentrated methanolic crude extract was suspended in 400 mL of distilled water:methanol (9:1, v/v) to ensure proper dissolution. The suspension was then sequentially partitioned with solvents of increasing polarity using a separatory funnel. Initially, the aqueous methanolic solution was extracted with petroleum ether (3 × 300 mL) to obtain the petroleum ether soluble fraction (PSF), targeting non-polar constituents such as lipids, sterols, and terpenoids. The remaining aqueous phase was subsequently partitioned with dichloromethane (3 × 300 mL) to yield the dichloromethane soluble fraction (DSF), followed by extraction with ethyl acetate (3 × 300 mL) to obtain the ethyl acetate soluble fraction (ESF). The final aqueous layer constituted the aqueous soluble fraction (ASF). Each fraction was separately concentrated under reduced pressure using a rotary evaporator at controlled temperature to yield PSF (16.1 g; 32.20% w/w), DSF (11.12 g; 22.24% w/w), ESF (12.18 g; 24.36% w/w), and ASF (7.32 g; 14.64% w/w). This systematic solvent partitioning enables efficient separation of phytoconstituents based on polarity, enhancing downstream biological and chemical analyses.

Compound isolation procedure

The PSF of the extract was utilized for compound separation. Gel permeation chromatography (GPC/SEC) was performed using Sephadex LH-20 (Sigma-Aldrich), and preparative thin-layer chromatography (PTLC) and thin-layer chromatography (TLC) were carried out on silica gel 60 F254 aluminum sheets (Merck, Germany) with a thickness of 0.25 mm. The TLC plates were examined under a UV lamp (UVGL-58, United States) at 254 nm and 365 nm. For visualization, the plates were sprayed with a vanillin-sulfuric acid solution and heated at 100°C for 5 minutes. Pure compounds were isolated via the PTLC method, and their purity was verified using spot TLC.

Compound identification procedure

The isolated compounds were subsequently analyzed using ^{1}H NMR spectroscopy. The spectra were recorded using Bruker spectrometers operating at 600 MHz. Samples were dissolved in deuterated solvents ($CDCl_3$ or MeOD) depending on solubility, and chemical shifts (δ) were reported in ppm relative to tetramethylsilane (TMS) or residual solvent peaks as internal standards [18]. Spectral acquisition parameters included typical settings such as 32–2000 scans, relaxation delays (D1 = 1–2 s), and spectral widths ranging from approximately 11,900–32,600 Hz, ensuring adequate signal resolution and sensitivity. For instance, high-resolution spectra were obtained on a Bruker 600 MHz instrument using $CDCl_3$ with

2000 scans and a relaxation delay of 2 s, while MeOD-based spectra were recorded with 64 scans and a relaxation delay of 1 s. All spectra were processed using exponential line broadening (LB = 0.30–1.0 Hz), followed by baseline correction and phase adjustment prior to integration. Integration was performed on baseline-corrected spectra to ensure accurate proton quantification, and peak assignments were made based on chemical shift, multiplicity, and comparison with published literature data.

In vitro activities

Antimicrobial activities. Disc diffusion (zone of inhibition) assay: The antimicrobial activity of the four fractions derived from the methanolic extract of *E. crassipes* flower was evaluated using the disc diffusion method [19]. Sterilized filter paper discs (6 mm diameter) impregnated with 100 µg of each test sample (CME, PSF, DSF, ESF, ASF) were placed onto nutrient agar plates pre-inoculated with bacterial and fungal strains. Positive controls included commercial antibiotic discs of Azithromycin, Amoxicillin, and Ciprofloxacin (30 µg/disc) and an antifungal disc of Fluconazole (30 µg/disc), while blank discs served as negative controls. The plates were inverted and stored at 4°C for 24 hours to allow even diffusion, followed by incubation at 37°C for an additional 24 hours. The zones of inhibition, reflecting antibacterial activity, were measured in millimeters [20]. The assay was conducted on clinically isolated strains of gram-positive bacteria (*Sarcina lutea*, *Bacillus megaterium*, *Staphylococcus aureus*, *Bacillus subtilis*, *Bacillus cereus*), gram-negative bacteria (*Vibrio mimicus*, *Pseudomonas aeruginosa*, *Salmonella typhi*, *Salmonella paratyphi*, *Escherichia coli*, *Shigella dysenteriae*, *Vibrio parahaemolyticus*), and fungal strains (*Aspergillus niger*, *Saccharomyces cerevisiae*, *Candida albicans*).

Minimum inhibitory concentration (MIC) assay: The minimum inhibitory concentration (MIC) of the extracts and fractions was determined against the tested microorganisms using a serial dilution method in a microtiter plate [21,22]. Initially, the test samples were dissolved in dimethyl sulfoxide (DMSO) to obtain a stock solution of 500 µL/mL. Subsequently, two-fold serial dilutions of the samples were prepared in sterile nutrient broth within the wells of a 96-well microtiter plate to obtain a range of decreasing concentrations. A microbial suspension was prepared and adjusted to an optical density of 0.01–0.1 at 600 nm, corresponding to approximately 10^7 cells/mL. Then, 10 µL of the microbial inoculum was added to each well containing 100 µL of sterile growth medium and the diluted test samples. The microtiter plates were incubated at 37 °C for 24 h for bacterial strains and at 25 °C for 48–72 h for fungal strains. After incubation, the wells were visually examined for microbial growth. The lowest concentration of the test sample that showed no visible growth of microorganisms was recorded as the MIC value, expressed in µL/mL.

Thrombolytic assay. The thrombolytic potential of the CME, PSF, DSF, ESF, and ASF of *E.crassipes* flower was assessed using streptokinase (SK) as the reference standard, following the protocol established by Prasad et al. (2006) [23]. Venous blood was collected from a healthy volunteer after obtaining written informed consent prior to sample collection. The experimental procedure was conducted in accordance with the ethical guidelines approved by the Institutional Ethics Review Committee of the State University of Bangladesh (Approval No. **2023-10-30/SUB/I-ERC/003**). The blood sample was collected on 10 Nov 2023. Six Eppendorf tubes were weighed, and 500 µL of blood was added to each tube. The tubes were incubated at 37°C for 45 minutes to allow clot formation. After coagulation, the serum was removed, and the tubes were reweighed to determine the clot weight. Subsequently, 100 µL of each fraction and the standard streptokinase solution were added to the respective tubes. The tubes were incubated again at 37°C for 90 minutes to promote clot lysis. After incubation, the released fluid was removed, and the tubes were weighed again to measure the weight change resulting from clot disruption. The percentage of clot lysis was calculated based on the weight difference before and after the lysis process.

The percentage of clot lysis was calculated using the following formula:

$$\% \text{ Clot Lysis } = \frac{\text{Weight of the Lysed Clot}}{\text{Weight of the Clot Before Lysis}} \times 100\ \%$$

In vivo analysis

Animal preparation. For the *in vivo* study, total 25 Swiss white mice of both sexes, aged four to five weeks, were procured from the Animal Resource Branch of the International Centre for Diarrheal Diseases and Research, Bangladesh (ICDDR, B). The mice were housed in polypropylene cages under controlled environmental conditions, including a 12-hour light-dark cycle, a temperature of 24 ± 2°C, and a relative humidity of 60–70%. They were fed ICDDR, B-formulated rodent food and provided water ad libitum. To ensure proper acclimatization and reduce stress, the mice were maintained under these conditions for at least four days before the experiments. All procedures adhered to ethical guidelines and regulations for the care and use of laboratory animals. The study followed the approved Animal Use Protocol from the Ethics Committee, in compliance with the US National Institutes of Health guidelines for the Care and Use of Laboratory Animals. Recommendations from the Federation of European Laboratory Animal Science Associations (FELASA) were also followed to minimize animal pain and stress.

The number of animals used in each experimental group (n = 4) was selected based on commonly applied group sizes in preliminary pharmacological screening studies, where the objective is to identify potential biological activity prior to more extensive confirmatory investigations. This approach also aligns with the ethical principle of Reduction within the 3R framework (Replacement, Reduction, and Refinement) for responsible animal use.

Mice were monitored for signs of pain or distress, including >20% body-weight loss, severe lethargy, inability to access food or water, unresponsive behavior, persistent piloerection, impaired mobility, labored breathing, convulsions, or abnormal posture. Any animal exhibiting these signs was immediately removed from the study and humanely euthanized using an intraperitoneal overdose of anesthesia (Ketamine HCl at 100 mg/kg and Xylazine at 7.5 mg/kg), as per established protocols [24,25].

Animals were observed every 4 hours during the first 24 hours after treatment and twice daily thereafter for changes in general behavior, food and water intake, posture, and locomotor activity. Detailed monitoring records were maintained throughout the experimental period to document any clinical signs of distress or abnormal physiological responses. No animals died during the study, and none reached the predefined humane endpoint criteria. The study protocol was approved by the Animal Ethics Committee of the State University of Bangladesh, Dhaka (**2023-10-30/SUB/A-ERC/005**). All personnel involved in animal handling and monitoring were trained in laboratory animal care, recognition of distress indicators, and approved euthanasia procedures. Following completion of the study, all surviving animals were monitored twice daily for an additional two months, during which no abnormal clinical signs, behavioral changes, or health complications were observed; the animals subsequently returned to their normal housing environment without any adverse outcomes. These observations further confirmed that the experimental procedures did not induce long-term physiological or behavioral distress in the animals.

Acute oral toxicity test. The methanol-soluble crude extract of *E. crassipes flower* was orally administered to mice at a high dose of 2000 mg/kg under controlled laboratory conditions, adhering to the fixed-dose method specified in OECD Guidelines 420 [4]. Throughout the acute toxicity assessment, animals were evaluated according to the same humane endpoints and monitoring schedule described above. During the 72-hour monitoring period, no allergic reactions, behavioral alterations (e.g., sedation or excitability), or fatalities were recorded. Consequently, doses of 200, 400 and 600 mg/kg (body weight, orally) were deemed safe and chosen for subsequent antidiarrheal activity evaluations.

Antidiarrheal assay. The antidiarrheal activity of various fractions of *E. crassipes* was evaluated using the castor oil-induced diarrhea model in mice, following established protocols [26]. Diarrhea was induced in each mouse by administering 1 mL of high-purity analytical-grade castor oil, and the total number of fecal excretions was recorded. The mice were divided into five groups: control, positive control, and three test groups, each consisting of four mice. The control group received 10 mL/kg of 1% Tween 80 in water orally, while the positive control group was given 5 mg/kg of loperamide orally. The test groups were administered *E. crassipes* extract fractions at doses of 200, 400 and 600 mg/kg body weight respectively. After treatment, diarrhea was induced with castor oil, and each mouse was placed in an

individual cage with hourly changes of the cage lining. The antidiarrheal effect was determined by comparing the test groups to the control group, with fecal counts recorded over a 4-hour observation period. The percentage inhibition of diarrhea was calculated using the formula:

$$\% \text{ Inhibition of Defecation} = \frac{\text{Mean Defecation by Control} - \text{Mean Defecation by Test Samples or Standard}}{\text{Mean Defecation by Control}} \times 100\ \%$$

Statistical analysis. The data were analyzed using GraphPad Prism 5.2 (GraphPad Software, Inc., La Jolla, CA, USA), and the results from the *in vivo* antidiarrheal experiments were expressed as mean ± standard error of the mean (SEM). Statistical significance was determined using one-way analysis of variance (ANOVA) and Dunnett's test. Significance levels were marked as *$p < 0.05$, **$p < 0.01$, and ***$p < 0.001$ [4].

Molecular docking

Software. Computational docking studies were performed on the metabolites identified from *C. affinis* whole plant extracts using established software tools, including PyRx, PyMoL 2.3, Discovery Studio 4.5, and Swiss PDB viewer [27].

Ligand preparation. For ligand preparation, the identified phytochemicals were retrieved from the PubChem database (https://pubchem.ncbi.nlm.nih.gov/), and their 3D structures were downloaded in SDF format. The 3D structures of reference compounds—Ciprofloxacin, amoxicillin, Loperamide, and Streptokinase—were also obtained. These ligands were imported into Discovery Studio 4.5, and the PM6 semi-empirical method was applied to optimize their structures for improved docking precision [28].

Target preparation. For receptor preparation, the 3D crystal structures of target proteins were sourced from the Protein Data Bank (RCSB PDB, https://www.rcsb.org) [29]. The selection of target proteins followed a rational design strategy based on the pharmacological activities evaluated experimentally in this study. For antidiarrheal activity, the kappa-opioid receptor (KOR) [PDB: 6VI4] [30] and human delta-opioid receptor (DOR) [PDB: 4RWD] [31] were selected because opioid receptors play important roles in regulating intestinal motility and secretion. For antimicrobial analysis, β-ketoacyl-ACP synthase 3 (KAS) [PDB: 1HNJ] [32] and Dihydrofolate reductase (DHFR) [PDB: 4M6J] [33] were chosen due to their essential involvement in bacterial fatty acid biosynthesis and folate metabolism, respectively, making them well-established antimicrobial drug targets. To explore thrombolytic potential, tissue plasminogen activator (TPA) [PDB: 1A5H] [29] was used because of its key role in fibrinolysis and clot degradation. The protein structures were processed in PyMOL 2.3 to remove water molecules and ligands/residues, and non-polar hydrogen atoms were added. Energy minimization was performed using Swiss PDB viewer [34]. Ligand-receptor interactions were analyzed using PyRx Autodock Vina, employing semiflexible docking methods. Proteins were prepared as macromolecules, and specific amino acids were selected to ensure precise ligand binding to the target sites [5]. The selection of target site and grid mapping of target receptors are shown as Table 1.

ADME/T analysis. In current drug discovery, computational methods that assess pharmacokinetic properties—absorption, distribution, metabolism, excretion, and toxicity (ADMET)—play a significant role in evaluating drug-like characteristics and bioavailability. These analyses are indispensable for exploring the pharmacological potential of new compounds (http://biosig.unimelb.edu.au/pkcsm/prediction). The Swiss ADME web tool (http://www.sib.swiss) was used to predict drug-likeness, applying Lipinski's rules and pharmacokinetic parameters. Lipinski's criteria state that a compound is likely to be orally active if it adheres to the following guidelines: a molecular weight below 500 atomic mass units (amu), up to 5 hydrogen bond donors, up to 10 hydrogen bond acceptors, and a lipophilicity value (LogP) not exceeding 5 [2].

Results

Phytochemicals

Compound 1 was a yellowish solid (4.9 mg), Rf = 0.61 (50% Ethyl acetate, 50% Toluene); the obtained ^{1}H NMR spectra showed consistency with the previously reported data presented in **Table 2**. The ^{1}H NMR spectrum ($CDCl_3$, 600 MHz)

Table 1. Selection of target site and grid mapping of target receptors for molecular docking of isolated compounds from PSF of methanolic extract of *E. crassipes* flower.

Target Activity	Receptor	Standard	Target binding sites	Reference	Grid box	
Antimicrobial	Dihydrofolate Reductase (DHFR) [PDB ID4M6J]	Ciprofloxacin (PubChem ID: 2764)	Asp 9, Phe 16, Ile 54, Gly 55, Ser 56, Ala 75, Lys 76, Glu 77, Leu 78, Tyr 91, Ile 92, Gly 93, Arg 117, Thr 118, Gln 119, Asp 120	[34]	Center	x = 3.30050538898
						y = −3.54749560527
						z = −18.6603468425
					Dimension	x = 20.8847111475
						y = 28.2427927367
						z = 27.1639553048
	Beta-ketoacyl-ACP synthases (KAS) [PDB ID:1HNJ]	Amoxicillin (PubChem ID: 33613)	Trp 32, Arg 36, Thr 37, Thr 81, Ala 109, Ala 110, Ala 111, Cys 112, Leu 142, Gly 152, Ile 155, Ile 156, Phe 157, Leu 189, Thr 190, Leu 191, Leu 205, Met 207, Gly 209, Asn 210, Val 212, Phe 213, Ala 216, Leu 220, His 244, Ala 246, Asn 247, Ile 250, Asn	[4]	Center	x = 29.0033635958
						y = 17.3175380047
						z = 31.5701285056
					Dimension	x = 26.5571751807
						y = 35.4261745701
						z = 23.0503334713
Antidiarrheal	Human Delta-Opioid Receptor (DOR) [PDB ID: 4RWD]	Loperamide (PubChem ID: 3955)	A chain- Val 62, Leu 65, Gly 66, Leu 69, Val 70, Phe 72, Gly 73, Tyr 77, Pro 315, Val 316, Ala 319, Phe 325, Cys 328, Phe 329, Gln 331, Leu 332	[5]	Center	x = −56.6815476866
						y = 1.83509476912
						z = 52.8777794668
					Dimension	x = 21.9977639041
						y = 18.6802030241
						z = 21.1327889808
	Kappa Opioid Receptor (KOR) [PDB ID: 6VI4]		B chain- Leu 103, Leu 107, Ser 136, Ile 137, Try 140, Ile 180, Trp 183, Leu 184, Ser 187, Ile 191, Leu 192 Ile 194, Val 195	[29]	Center	x = 54.4225497657
						y = −50.4523701153
						z = −16.3056618844
					Dimension	x = 16.2392828969
						y = 28.2473102176
						z = 18.0419317341
Thrombolytic	Tissue Plasminogen Activator (TPA) [PDB ID: 1A5H]	Streptokinase (PubChem ID: 482240142)	Arg 39, Leu 41, Cys 42, His 57, Cys 58, Gln 60, Glu 60A, Phe 60C, Tyr 99, Tyr 151, Asp 189, Ala 190, Cys 191, Gln 192, Gly 193, Ser 195, Ile 213, Ser 214, Trp 215, Gly 216, Leu 217, Gly 219, Val 224, Pro 225, Gly 226, Val 227, and Tyr 228	[29]	Center	x = 5.31220314201
						y = 35.0614579238
						z = 49.2471129809
					Dimension	x = 27.1580470485
						y = 24.29842386
						z = 30.4915813269

https://doi.org/10.1371/journal.pone.0351085.t001

showed peak at δ 7.867 (2H, d J = 7.2 Hz, H-2′), δ 6.43 (2H, d J = 7.8 Hz, H-3′), δ 6.467 (1H, s, H-8), and δ 6.217 (1H, s, H-6) (Fig 1).

Compound 2 was a yellowish solid (6.1 mg), Rf = 0.54 (80% Ethyl acetate, 20% Toluene); The spectral profile obtained from ^{1}H NMR analysis agrees with the previously documented data given in Table 2. The ^{1}H NMR spectrum (MeOD-d4, 600 MHz) showed peak at δ 6.214 (1H, s, H-6), δ 6.499 (1H, s, H-8), δ 6.548 (1H, s, H-3), δ 6.9 (1H, d = 7.8 Hz, H-5′), and δ 7.3825 (2H, d J = 9 Hz, H-2′, H-6′) (Fig 2).

Compound 3 was crystalline solid (5.2 mg), Rf = 0.23 (07% Ethyl acetate, 93% Toluene); the observed ^{1}H NMR resonances aligned with previously published values, as illustrated in Table 2. The ^{1}H NMR spectrum ($CDCl_3$, 600 MHz) illustrated peak at δ 3.52 (1H, m, H-3), δ 5.35 (1H, br s, H-6), δ 0.68 (1H, s, H-18), δ 1.01 (1H, s, H-19), δ 5.12 (1H, dd, J = 9

Table 2. The ^{1}H NMR of the isolated compounds from PSF of methanolic extract of flower of *E. crassipes* compared with reference spectroscopic data.

Compound No	Compound Name	Position	H-NMR Values (δ IN PPM)	Reference Values (δ IN PPM)	Reference
			$CDCl_3$, 600 MHz	**CD_3OD, 400 MHz**	
1	3,5,7, 4'-Tetrahydroxyflavone (Kaempferol)	H-2′	7.87 (d, 7.2, 2H)	8.05(2H, d, J08.5 Hz)	[35]
		H-3′	6.94 (d, 7.8, 2H)	6.88 (2H, d, J08.5 Hz)	
		H-8	6.47 (s, 1H)	6.35 (1H,s)	
		H-6	6.22 (s, 1H)	6.15(1H,s)	
			MeOD-d4, 600 MHz	**CD_3OD, 500 MHz**	
2	3',4',5,7-Tetrahydroxyflavone (Luteolin)	H-6	6.21 (s, 1H)	6.19 (1H, d, J = 2.0 Hz)	[36]
		H-8	6.49 (s, 1H)	6.42 (1H, d, J = 2.0 Hz)	
		H-3	6.55 (s, 1H)	6.52 (1H,s)	
		H-5′	6.90 (d, J = 7.8, 1H)	6.88 (1H, d, J = 8.5 Hz)	
		H-2′, H-6′	7.38 (d, J = 9, 2H)	7.36 (2H, m)	
			$CDCl_3$ at 600 MHz	**500 MHz, $CDCl_3$**	
3	Stigmasterol	H-3	3.52 (m, 1H)	3.32 (m, 1H)	[37]
		H-6	5.35 (br s, 1H)	5.35 (d, 6.0, 1H)	
		H-18	0.68 (s, 3H)	0.73 (s, 3H)	
		H-19	1.01 (s, 3H)	1.02 (s, 3H)	
		H-22	5.12 (dd, 9, 7.2, 1H)	5.05 (dd, 8.5, 15, 1H)	
		H-23	5.02 (dd, 9, 8.4, 1H)	4.95 (dd, 8.5, 15, 1H)	
		H-26	0.81 (d, 7.2, 3H)	0.83 (d, 3H)	
		H-27	0.79 (d, 7.8, 3H)	0.81 (d, 3H)	
		H-29	0.84 (d, 7.8, 3H)	0.86 (d, 3H)	
			MeOD-d4, 600 MHz	**DMSO, 400 MHz**	
4	4- Carboxybenzyl alcohol	H-2, H-6	7.87 (d, 9, 2H)	7.90 (d, 8.2 2H)	[38]
		H-3, H-5	6.81 (d, 8.4, 2H)	7.42 (d, 8.3, 2H)	
			4.58 (s, 2H)	4.57 (s, 2H)	
			$CDCl_3$, 600 MHz	**DMSO, 400 MHz**	
5	4-methoxybenzaldehyde	H-2, H-6	7.41 (2H, d, J = 7.2 Hz)	7.87 (2H, d, J = 8.6 Hz)	[39]
		H-3, H-5	6.79 (2H, d, J = 7.8 Hz)	7.12 (2H, d, J = 8.6 Hz)	
			3.83 (3H, s)	3.86 (3H, s)	
				9.87 (3H, s)	

https://doi.org/10.1371/journal.pone.0351085.t002

Hz, 7.2 Hz, H-22), δ 5.02 (1H, dd, J = 9 Hz, 8.4 Hz, H-23), δ 0.81 (3H, d, J = 7.2 Hz, H-26), δ 0.79 (3H, d, J = 7.8 Hz, H-27), and δ 0.84 (3H, d, J = 7.8 Hz, H-29) (Fig 3).

Compound 4 was white solid (3.1 mg), Rf = 0.59 (60% Ethyl acetate, 40% Toluene); the ^{1}H NMR signals observed for the compound correspond well with the reference data presented in Table 2. The ^{1}H NMR spectrum (MeOD-D4, 600 MHz) showed peak at 7.87 (2H, d J = 9 Hz), 6.81 (2H, d J = 8.4 Hz), and 4.58 (2H, s) (Fig 4).

Compound 5 was pale yellow oily liquid (4.7 mg), Rf = 0.54 (50% Ethyl acetate, 50% Toluene); the obtained ^{1}H NMR spectral data matched closely with those previously reported and listed in Table 2. The ^{1}H NMR spectrum (MeOD-D4, 600 MHz) showed peak at 7.41 (2H, d, J = 7.2 Hz), 6.79 (2H, d, J = 7.8 Hz), and 3.83 (3H, s) (Fig 5).

Antimicrobial activities. Disc diffusion method (zone of inhibition): The antimicrobial results revealed that CME displayed broad-spectrum inhibitory activity (Table 3). Among Gram-positive organisms, substantial activity was observed against *Bacillus cereus* (10.00 ± 0.82 mm), *Bacillus subtilis* (20.33 ± 1.25 mm), and *Staphylococcus aureus* (7.67 ± 1.25 mm). In Gram-negative organisms, the extract inhibited the growth of *Salmonella paratyphi*

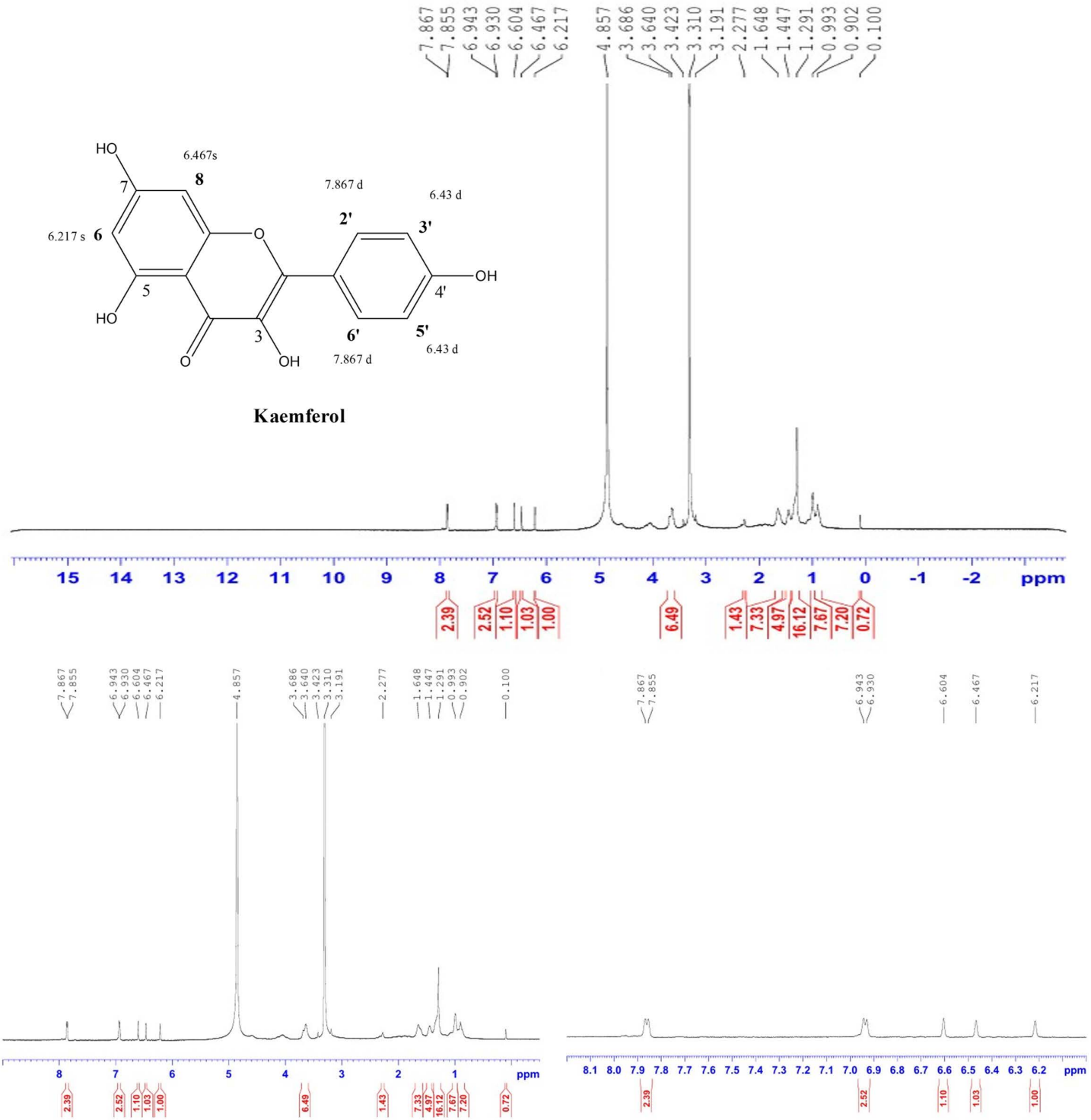


Fig 1. ^{1}H NMR spectrum of 3,5,7,4'-Tetrahydroxyflavone (Kaempferol) isolated from PSF of methanolic extract of flower of *E. crassipes*.

https://doi.org/10.1371/journal.pone.0351085.g001

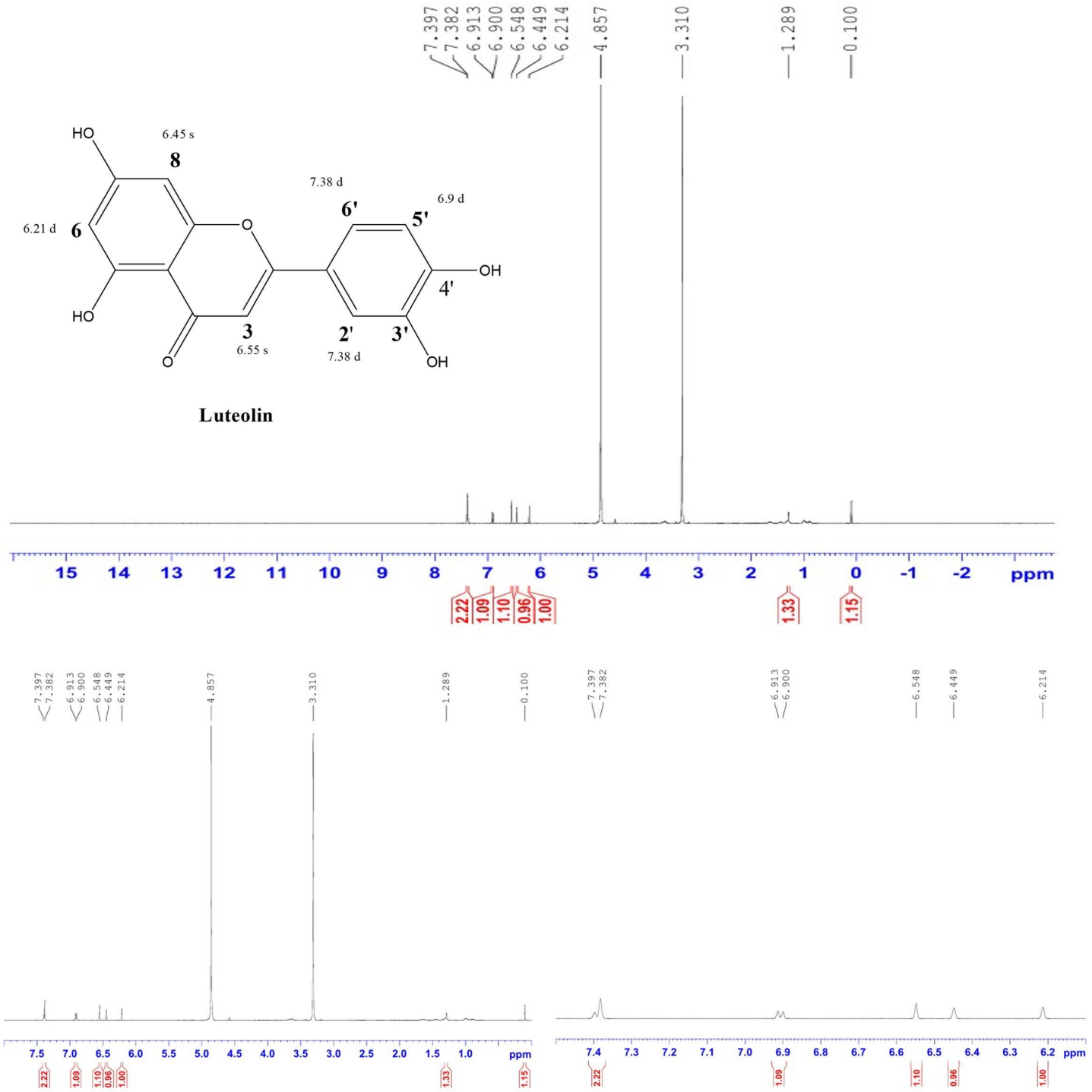


Fig 2. ^{1}H NMR spectrum of 3',4',5,7-Tetrahydroxyflavone (Luteolin) isolated from PSF of methanolic extract of flower of *E. crassipes*.

https://doi.org/10.1371/journal.pone.0351085.g002

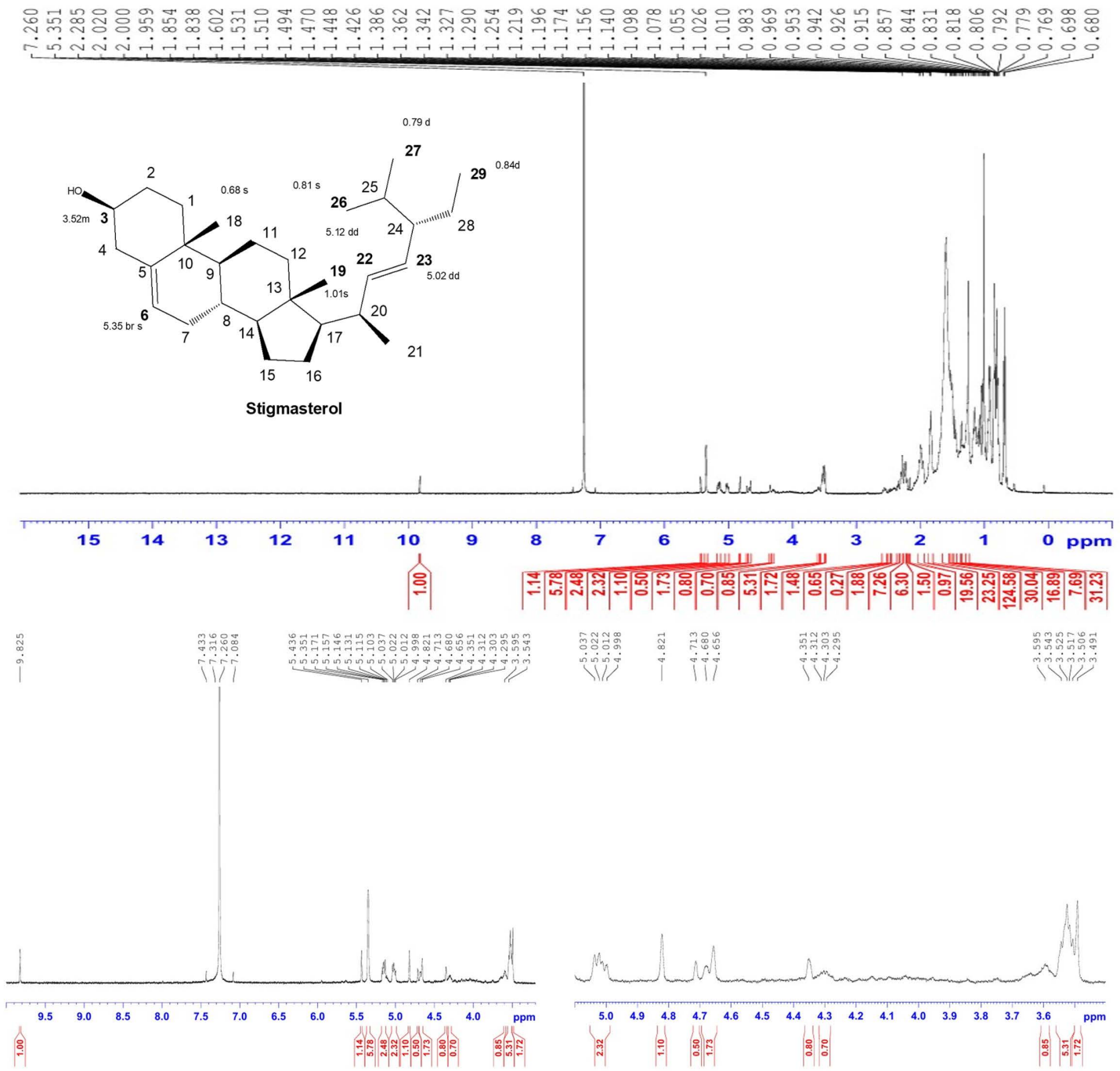


Fig 3. ^{1}H NMR spectrum of Stigmasterol isolated from PSF of methanolic extract of flower of *E. crassipes*.

https://doi.org/10.1371/journal.pone.0351085.g003

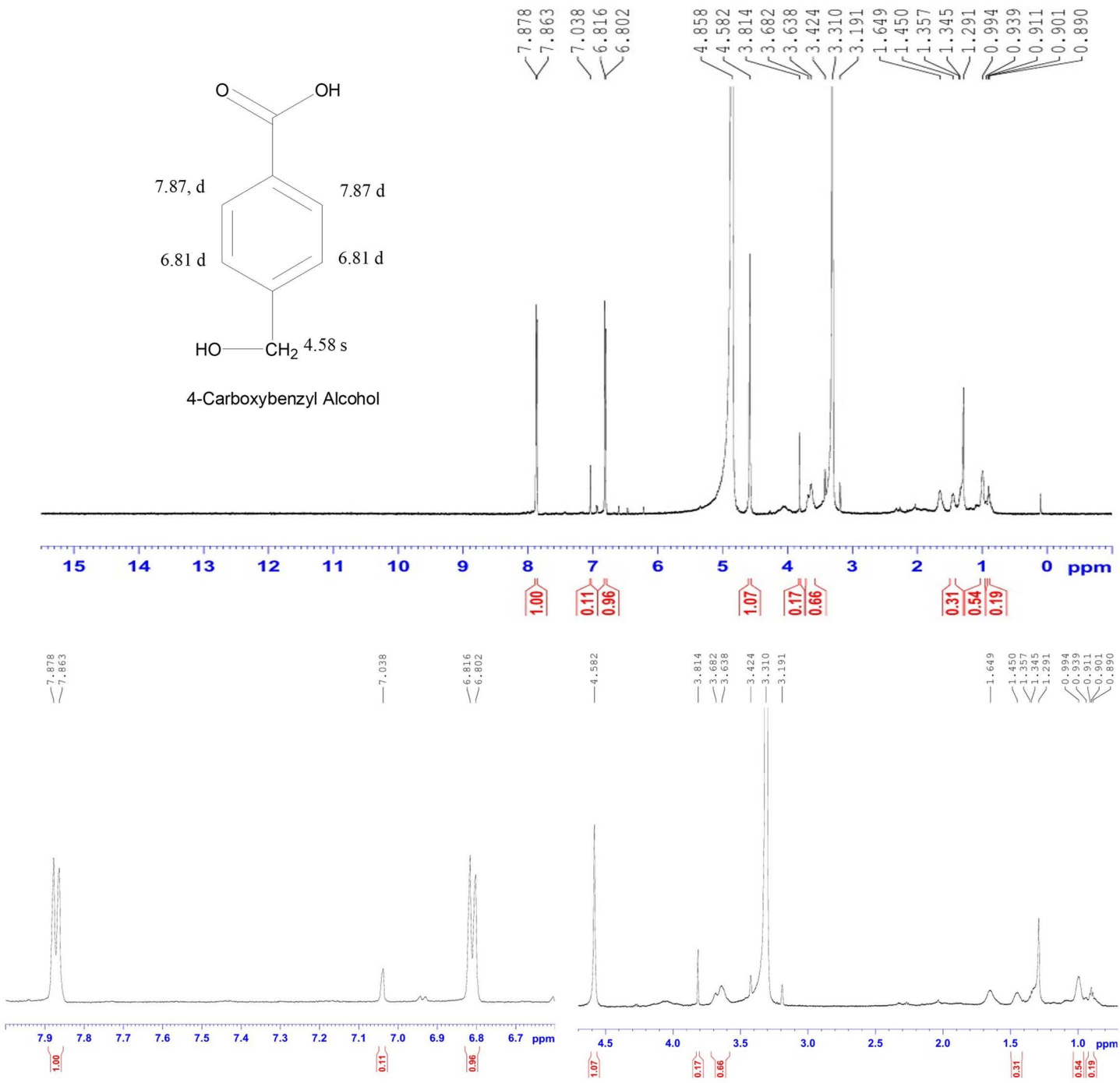


Fig 4. ^{1}H NMR spectrum of 4-Carboxybenzyl alcohol isolated from PSF of methanolic extract of flower of *E. crassipes*.

https://doi.org/10.1371/journal.pone.0351085.g004

(9.00 ± 0.82 mm), *Vibrio parahaemolyticus* (9.67 ± 0.47 mm), and *Shigella dysenteriae* (8.33 ± 0.47 mm). Additionally, antifungal effects were evident against *Candida albicans* (7.00 ± 0.82 mm), *Saccharomyces cerevisiae* (9.00 ± 0.82 mm), and *Aspergillus niger* (11.67 ± 1.70 mm). Although the inhibitory zones were smaller than those produced by the

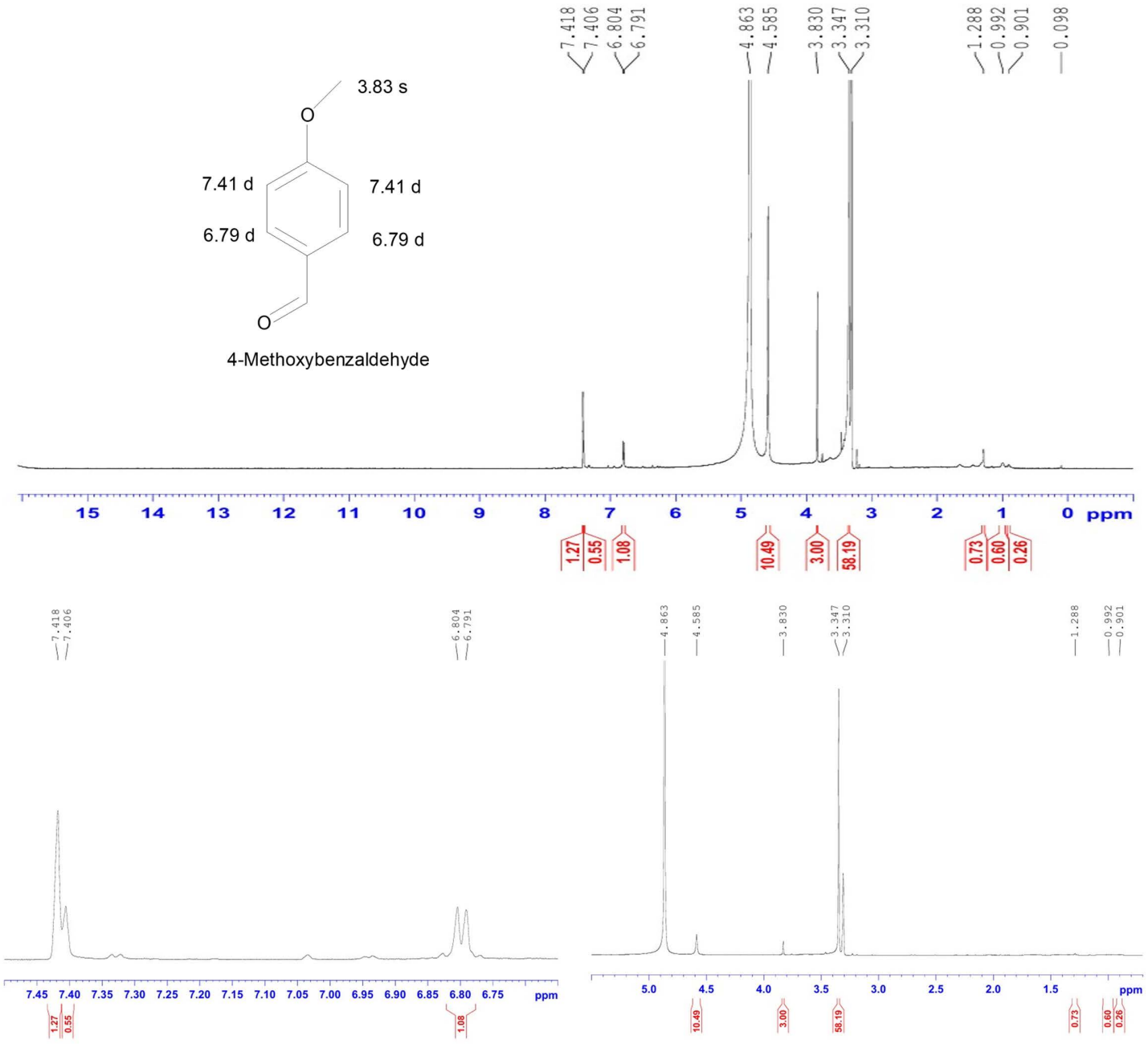


Fig 5. ^{1}H NMR spectrum of 4-methoxybenzaldehyde isolated from PSF of methanolic extract of flower of *E. crassipes*.

https://doi.org/10.1371/journal.pone.0351085.g005

standard drugs ciprofloxacin (for bacteria) and fluconazole (for fungi), the extract's effects were nonetheless noteworthy.

Minimum inhibitory concentration (MIC) assay: Among the Gram-positive bacteria, the DSF exhibited the most potent activity, particularly against *B. subtilis* and *S. aureus*, with the lowest MIC value of 15.6 µL/mL. The CME also demonstrated notable activity against *B. subtilis* (15.6 µL/mL) and *S. lutea* (62.5 µL/mL). In contrast, the

Table 3. Antimicrobial activity of different extracts of *Eichhornia crassipes* flower determined by disc diffusion method (zone of inhibition, mm) and minimum inhibitory concentration (MIC, µL/mL).

Test Microorganisms	Zone of Inhibition (mm)						Minimum Inhibitory Concentration (µL/mL)				
	Standard	CME	PSF	DSF	ESF	ASF	CME	PSF	DSF	ESF	ASF
Gram Positive Bacteria											
Bacillus cereus	42.33 ± 0.47	10.00 ± 0.82	4.67 ± 0.94	7.33 ± 0.47	8.67 ± 0.94	3.00 ± 0.00	62.5	>500	250	250	>500
Bacillus megaterium	32.00 ± 0.82	9.33 ± 0.47	6.67 ± 1.70	8.67 ± 0.47	7.67 ± 0.94	0.00 ± 0.00	125	500	125	250	>500
Bacillus subtilis	40.67 ± 0.47	20.33 ± 1.25	5.67 ± 0.94	15.00 ± 0.82	10.00 ± 0.82	4.67 ± 0.47	15.6	500	31.2	125	>500
Staphylococcus aureus	42.67 ± 1.25	7.67 ± 1.25	9.67 ± 1.25	17.33 ± 0.47	14.67 ± 1.25	0.00 ± 0.00	250	125	15.6	62.5	>500
Sarcina lutea	40.00 ± 0.82	11.00 ± 1.63	8.33 ± 0.47	11.00 ± 0.82	11.00 ± 1.63	0.00 ± 0.00	62.5	125	62.5	62.5	>500
Gram Negative Bacteria											
Salmonella paratyphi	43.00 ± 0.82	9.00 ± 0.82	8.00 ± 0.82	8.67 ± 0.47	8.67 ± 1.70	2.33 ± 0.47	125	250	125	125	>500
Salmonella typhi	42.67 ± 0.94	8.33 ± 0.47	12.67 ± 1.25	9.00 ± 0.82	4.33 ± 0.47	0.00 ± 0.00	125	62.5	125	>500	>500
Vibrio parahaemolyticus	41.33 ± 0.47	9.67 ± 0.47	4.67 ± 0.94	8.33 ± 0.94	8.67 ± 0.58	2.67 ± 0.47	125	>500	125	125	>500
Escherichia coli	40.33 ± 1.25	12.67 ± 1.25	8.33 ± 0.94	6.67 ± 1.15	6.67 ± 0.94	0.00 ± 0.00	62.5	250	500	500	>500
Vibrio mimicus	37.00 ± 1.63	11.33 ± 0.47	10.33 ± 1.25	7.33 ± 0.47	6.00 ± 0.00	0.00 ± 0.00	62.5	125	250	500	>500
Shigella dysenteriae	38.00 ± 0.82	8.33 ± 0.47	10.67 ± 1.25	9.67 ± 0.94	7.33 ± 1.53	5.00 ± 0.82	125	62.5	125	250	500
Pseudomonas aeruginosa	39.00 ± 2.16	11.67 ± 0.47	8.67 ± 0.47	8.00 ± 0.82	8.00 ± 0.82	0.00 ± 0.00	62.5	125	250	250	>500
Shigella boydii	40.67 ± 0.47	11.67 ± 0.94	9.33 ± 1.25	9.33 ± 0.47	11.67 ± 0.47	0.00 ± 0.00	62.5	125	125	125	>500
Fungi											
Saccharomyces cerevisiae	36.33 ± 1.25	9.00 ± 0.82	7.67 ± 0.47	8.00 ± 0.82	6.67 ± 0.47	6.33 ± 0.47	125	250	250	500	500
Candida albicans	40.00 ± 0.82	7.00 ± 0.82	6.67 ± 0.47	3.67 ± 0.47	7.67 ± 1.25	4.00 ± 0.82	250	500	>500	250	>500
Aspergillus niger	48.00 ± 2.16	11.67 ± 1.70	4.00 ± 0.82	7.67 ± 0.47	11.00 ± 0.82	5.67 ± 0.47	62.5	>500	250	62.5	>500

Zone of Inhibition results are expressed as Mean ± SD. For Gram positive and negative bacteria Ciprofloxacin used as standard, and for fungi Fluconazole used as standard.

https://doi.org/10.1371/journal.pone.0351085.t003

ASF showed no significant inhibition against Gram-positive bacteria, with MIC values exceeding 500 µL/mL in all cases.

For Gram-negative bacteria, moderate antimicrobial activity was observed across CME, PSF, and DSF fractions. The lowest MIC values (62.5 µL/mL) were recorded for CME against *E. coli*, *V. mimicus*, and *P. aeruginosa*. The PSF exhibited selective activity, with an MIC of 62.5 µL/mL against *S. typhi* and *S. dysenteriae*. However, higher MIC values (≥250 µL/mL) were generally observed for ESF and ASF, indicating comparatively weaker activity of these fractions against Gram-negative organisms.

In antifungal assays, the CME fraction showed moderate activity against *A. niger* (62.5 µL/mL), whereas other fractions demonstrated limited efficacy. The DSF fraction exhibited moderate inhibition against *S. cerevisiae* (250 µL/mL), while most other combinations, particularly ASF, showed MIC values of ≥500 µL/mL, suggesting minimal antifungal potential.

Overall, the results indicate that the DSF and CME fractions possess comparatively stronger antimicrobial activity, while PSF and ESF exhibit moderate, organism-specific effects, and ASF remains largely inactive. The observed variability in MIC values highlights the influence of solvent polarity and phytochemical composition on antimicrobial efficacy.

Thrombolytic activities

The thrombolytic activity of *E. crassipes* flower extracts and their fractions was evaluated *in vitro* and expressed as percentage of clot lysis (**Fig 6**). The blank control produced 31.28% clot lysis, whereas the reference drug SK showed 66.67% clot lysis, confirming the validity of the assay. Among the tested samples, CME exhibited 17.68% clot lysis,

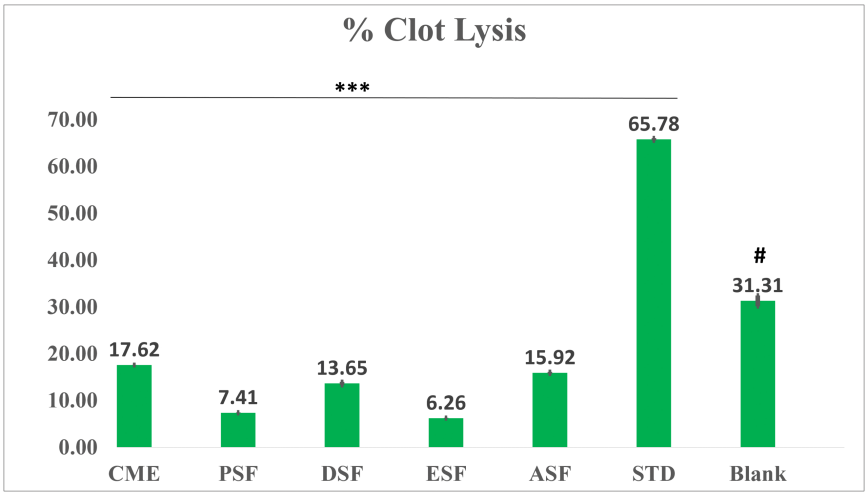


Fig 6. Thrombolytic activities of different fraction of methanolic extract of flower of *E. crassipes*.

https://doi.org/10.1371/journal.pone.0351085.g006

followed by ASF (15.80%), DSF (13.32%), PSF (7.40%), and ESF (6.23%). Overall, the extracts and fractions demonstrated measurable but moderate thrombolytic activity compared with the standard SK. These findings suggest that the thrombolytic constituents of *E. crassipes* flowers are more concentrated in the ethyl acetate fraction.

Antidiarrheal activities

The antidiarrheal activity of CME extract was evaluated at three doses (200, 400, and 600 mg/kg) compared to a standard drug and control group over a 4-hour period (Table 4). The control group showed a progressive increase in diarrheal count from 1.00 ± 0.41 at 1 hour to 4.50 ± 0.50 at 4 hours. CME 200 mg/kg demonstrated moderate reduction in diarrheal counts, with 50% reduction at 1 hour but no effect at 3 hours. CME 400 mg/kg showed stronger activity, with 75% reduction at 1 hour and statistically significant 77.78% reduction at 2 hours ($p < 0.05$). The highest dose of CME 600 mg/kg produced the most pronounced effects, completely preventing diarrhea at 1 hour (100% reduction) and maintaining significant reductions of 77.78% at 2 hours ($p < 0.05$), 55.56% at 3 hours, and 38.89% at 4 hours. The standard drug exhibited comparable efficacy to CME 600 mg/kg, showing 100% reduction at 1 hour and maintaining statistically significant 61.11% reduction at 4 hours ($p < 0.05$).

Molecular-docking

Molecular docking investigations of the isolated constituents from the PSF of *Eichhornia crassipes* flower demonstrated diverse binding behaviors toward antimicrobial, antidiarrheal, and thrombolytic protein targets (Table 5, Figs 7–11). Stigmasterol emerged as the most active compound, with docking scores of –8.4 (DHFR), –7.5 (KAS), –8.4 (delta-opioid receptor), –10.3 (kappa-opioid receptor), and –7.7 kcal/mol (tPA). Luteolin also displayed strong and consistent affinities across all tested proteins, ranging between –7.5 and –9.1, while Kaempferol recorded moderately high interactions spanning –6.8 to –8.4. In contrast, the simpler phenolic molecules showed weaker binding tendencies; 4-carboxybenzyl alcohol yielded values between –5.4 and –6.5, and 4-methoxy benzene demonstrated the lowest scores (–4.3 to –5.2).

The performance of the phytochemicals was comparable with standard reference ligands. Ciprofloxacin and amoxicillin interacted strongly with antimicrobial proteins (–8.2 and –7.1, respectively), loperamide showed excellent binding to opioid receptors (–8.5 and –9.1), while streptokinase exhibited a lower affinity (–5.8) with tPA compared to Stigmasterol and Luteolin. These results indicate that the sterols and flavonoids from *E. crassipes* may interact with the selected targets

Table 4. Anti-diarrheal activites of methanolic crude extract of flower of *E. crassipes* through Castor oil induced diarrheal assay.

Groups	Average diarrheal count				% Reduction in diarrheal count			
	1 h	2 h	3 h	4 h	1 h	2 h	3 h	4 h
Control	1.00 + 0.41	2.25 + 0.48	2.25 + 0.48	4.50 + 0.50	–	–	–	–
CME 200	0.50 + 0.50	1.75 + 0.85	2.25 + 1.11	4.00 + 0.82	50.00	22.22	0.00	11.11
CME 400	0.25 + 0.25	0.50 + 0.50*	2.00 + 0.41	3.75 + 0.48	75.00	77.78	11.11	16.67
CME 600	0.00	0.50 + 0.50*	1.00 + 1.00	2.75 + 1.18	100.00	77.78	55.56	38.89
STD	0.00	0.75 + 0.25*	1.25 + 0.48	1.75 + 0.63*	100.00	66.67	44.44	61.11

Results express as (Average ± SEM) while N = 4 and levels of significance were denoted as *p < 0.05, **p < 0.01, and ***p < 0.001.

https://doi.org/10.1371/journal.pone.0351085.t004

Table 5. Molecular docking of isolated compounds from PSF of methanolic extract of flower of *E. crassipes* against different target receptors.

SL. NO	Compound Name	Pub chem ID	Antimicrobial		Antidiarrheal		Thrombolytic
			Dihydrofolate Reductase (DHFR) [PDB ID4M6J]	Beta-ketoacyl-ACP synthases (KAS) [PDB ID:1HNJ]	Human Delta-Opioid Receptor (DOR) [PDB ID: 4RWD]	Kappa Opioid Receptor (KOR) [PDB ID: 6VI4]	Tissue Plasmino-gen Activator (TPA) [PDB ID: 1A5H]
1	Kaempferol	5280863	−7.8	−6.8	−8.4	−8.4	−7.6
2	Luteolin	5280445	−8.1	−7.5	−8.1	−9.1	−8
3	Stigmasterol	5280794	−8.4	−7.5	−8.4	−10.3	−7.7
4	4-Carboxybenzyl alcohol	7009454	−5.4	−5.6	−6.5	−5.7	−6.1
5	4-Methoxy benzene	7519	−4.3	−4.6	−5.2	−4.9	−5.2
STD	Ciprofloxacin	2764	−8.2				
	Amoxicillin	33613		−7.1			
	Loperamide	3955			−8.5	−9.1	
	Streptokinase	482240142					−5.8

https://doi.org/10.1371/journal.pone.0351085.t005

with comparable predicted affinities; however, these results represent computational estimates and require experimental validation.

Discussion

The ^{1}H NMR spectrum (CDCl3, 600 MHz) of **Compound 1** provides clear and distinct signals that help confirm its flavonoid structure. The doublet at 7.867 ppm (J = 7.2 Hz) corresponds to the two protons at C2′ on the B-ring, indicating that these protons are adjacent to each other in an ortho relationship. Similarly, the doublet at 6.43 ppm (J = 7.8 Hz) is assigned to the two protons at C3′ on the B-ring, which are also in an ortho relationship, as indicated by the similar coupling constant. These signals suggest that the B-ring of **5,7,4'-Tetrahydroxyflavone** is symmetrically substituted with protons at positions 2′ and 3′. The singlet at 6.467 ppm corresponds to the proton at C8 on the A-ring, which is isolated and does not couple with adjacent protons, as expected for a proton in this position. Another singlet at 6.217 ppm is assigned to the proton at C6, which is also isolated and does not show coupling with nearby protons. This further supports the typical pattern for a flavonoid structure, where protons on the A-ring and B-ring exhibit distinct coupling behaviors. The overall pattern of signals, with doublets for the protons on the B-ring and singlets for those on the A-ring, is consistent with the known proton environments of **3,5,7,4'-Tetrahydroxyflavone** or **Kaempferol**. This confirms that Kaempferol possesses a hydroxylated B-ring and a conjugated A-ring, as well as a typical flavonoid structure.

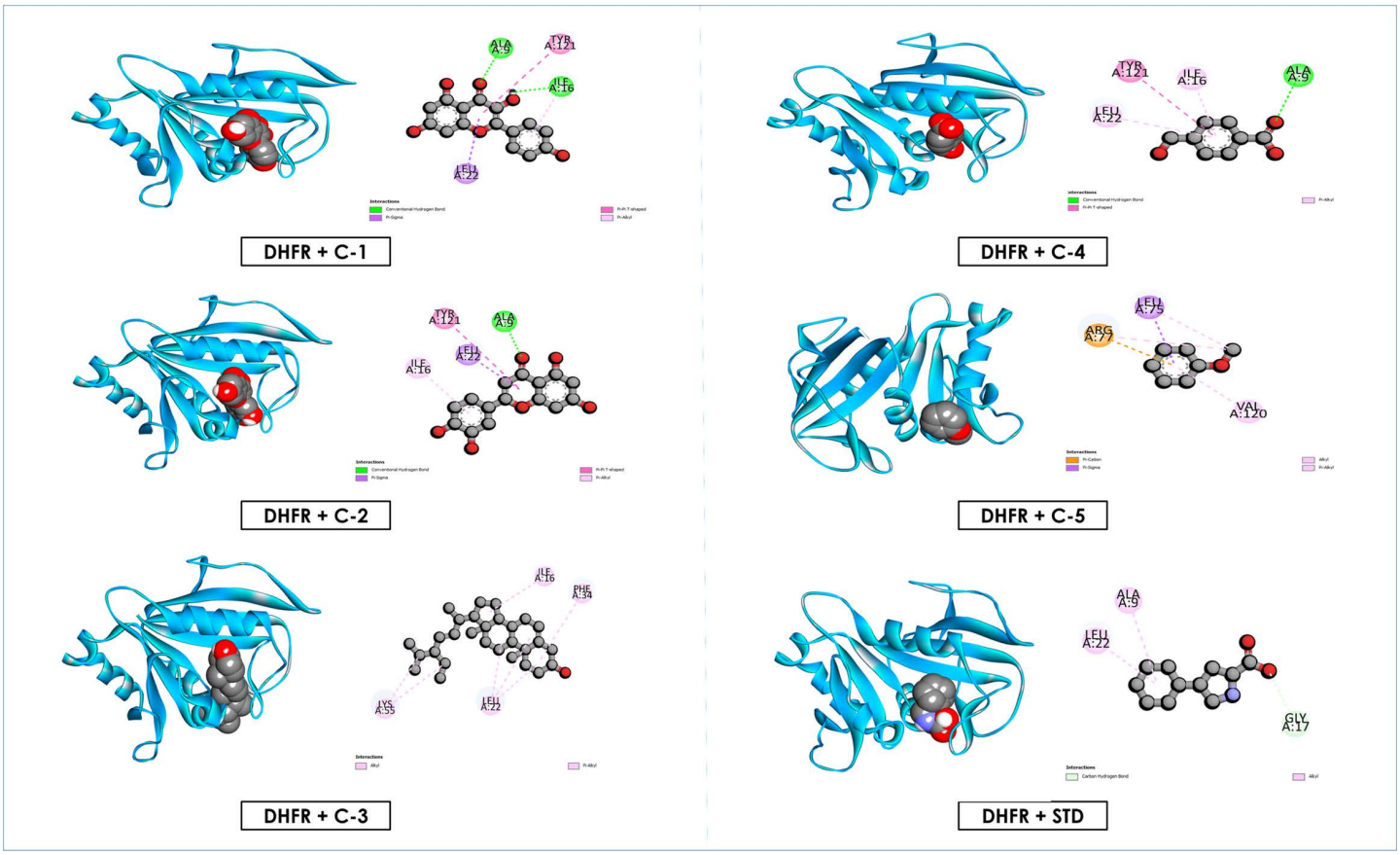


Fig 7. Molecular docking interactions of the isolated compounds with dihydrofolate reductase (DHFR). The figure illustrates both 3D binding conformations within the active site pocket and corresponding 2D interaction maps, highlighting key interactions such as hydrogen bonding, hydrophobic contacts, and π–alkyl interactions between the ligands and amino acid residues located in the DHFR catalytic region.

https://doi.org/10.1371/journal.pone.0351085.g007

The ^{1}H NMR spectrum (MeOD-d_4, 600 MHz) of **Compound 2** reveals several characteristic signals that confirm its flavonoid structure. The singlet at 6.214 ppm corresponds to the aromatic proton H-6, located on the A-ring of the flavonoid. The absence of coupling suggests that this proton has no neighboring protons, consistent with the substitution pattern of the ring. The singlet at 6.499 ppm is assigned to H-8, another proton on the A-ring, indicating a similar isolated environment. The difference in chemical shifts between H-6 and H-8 is influenced by the electron density distribution within the ring system. The singlet at 6.548 ppm is attributed to H-3, positioned within the central ring system of the flavonoid. This proton is strongly influenced by the extended conjugation of the structure, which leads to its characteristic downfield shift. The lack of splitting further supports its placement, as it is not adjacent to another proton. The doublet at 6.9 ppm (J = 7.8 Hz) corresponds to H-5′, located on the B-ring of the flavonoid. The coupling constant of 7.8 Hz suggests an ortho relationship between H-5′ and an adjacent proton, reinforcing the expected substitution pattern of the B-ring. The doublet at 7.3825 ppm (J = 9 Hz) is assigned to H-2′ and H-6′, which are also in an ortho arrangement on the B-ring. The coupling constant of 9 Hz supports their close positioning, confirming the expected connectivity of the ring system. Together, these signals confirm the structure of **3',4',5,7-Tetrahydroxyflavone** or **Luteolin**, a hydroxylated flavonoid with a defined arrangement of protons on both the A-ring and B-ring. The pattern of singlets and doublets aligns with the expected electronic environment and substitution pattern, reinforcing the molecular framework of **Luteolin**.

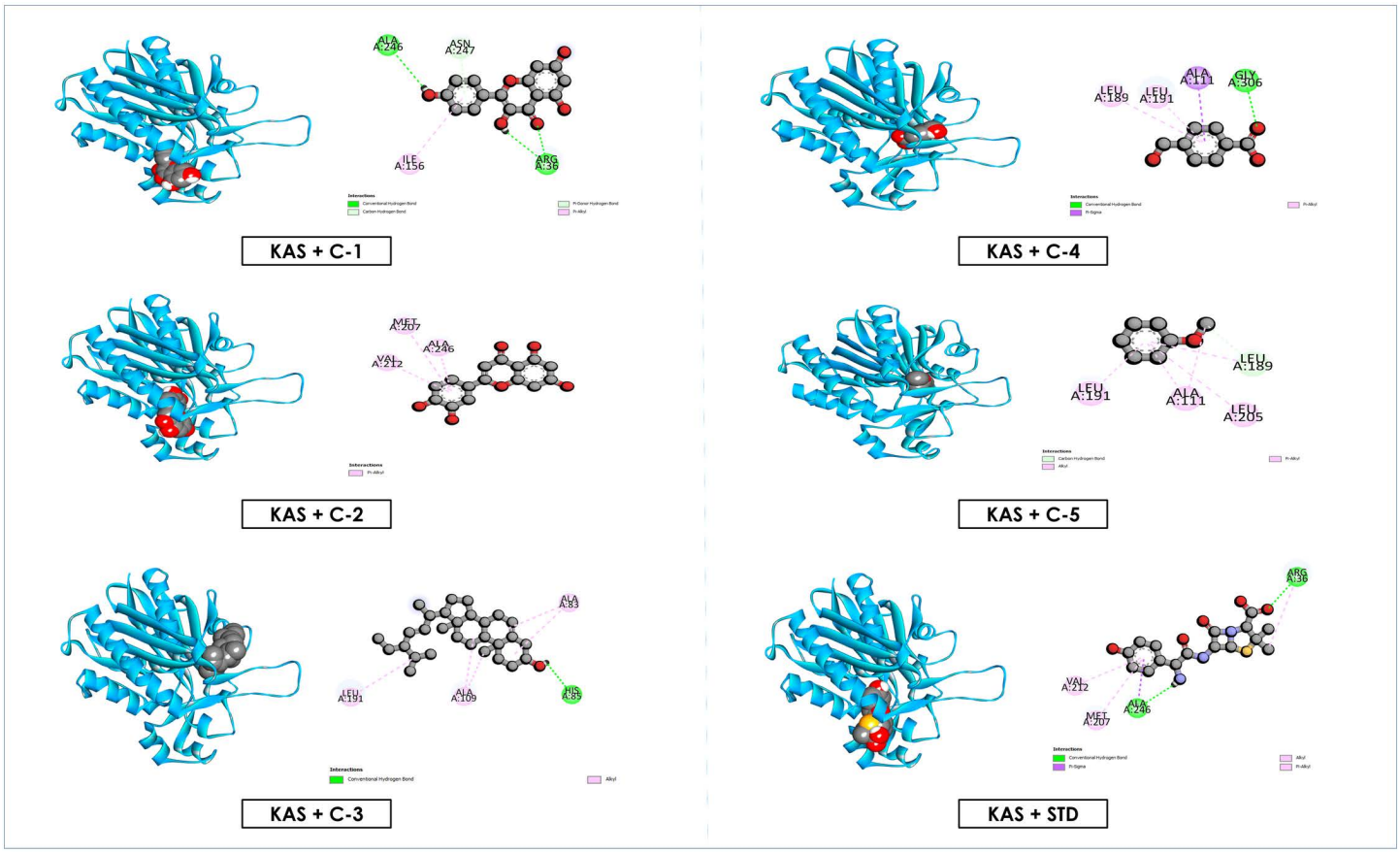


Fig 8. Docking interactions of the isolated compounds with β-ketoacyl-ACP synthase (KAS). The 3D docking poses and 2D interaction diagrams show the orientation of the ligands within the KAS active site and indicate important hydrogen bonds and hydrophobic interactions with catalytic residues, suggesting potential binding stability.

https://doi.org/10.1371/journal.pone.0351085.g008

The ^{1}H NMR spectrum ($CDCl_3$, 600 MHz) of **Compound 3** exhibits characteristic signals confirming its steroidal framework, hydroxyl functionality, and unsaturated side chain. A multiplet at δ 3.517 ppm is assigned to H-3, indicating the presence of a hydroxyl (-OH) group at C-3, a typical feature of sterols. The broad singlet at δ 5.351 ppm corresponds to H-6, confirming a double bond between C-5 and C-6 in the steroid nucleus. The singlets at δ 0.680 and δ 1.010 ppm correspond to H-18 and H-19, which are characteristic methyl groups in the sterol core. The side-chain double bond is confirmed by double doublets at δ 5.124 (J = 9, 7.2 Hz) and δ 5.017 (J = 9, 8.4 Hz), attributed to H-22 and H-23, indicating a double bond between C-22 and C-23. The aliphatic side-chain methyl groups appear as doublets at δ 0.812 (J = 7.2 Hz, H-26), δ 0.786 (J = 7.8 Hz, H-27), and δ 0.838 (J = 7.8 Hz, H-29), confirming the presence of an isopropyl terminal at the end of the side chain. The observed chemical shifts, coupling constants, and splitting patterns are consistent with the structure of **Stigmasterol**, confirming its hydroxylated sterol core, double bonds at C-5, C-6, C-22, and C-23, and a branched aliphatic side chain.

The ^{1}H-NMR spectrum of **Compound 4**, isolated from the dichloromethane fraction of *Eichhornia crassipes* flower, was recorded in MeOD-d4 at 600 MHz. The spectrum displayed a well-resolved pattern characteristic of a para-substituted benzene ring. Two doublets were observed at δ 7.87 ppm (d, J = 9 Hz, 2H) and δ 6.81 ppm (d, J = 8.4 Hz, 2H), corresponding to the aromatic protons at positions H-2/H-6 and H-3/H-5, respectively. The coupling constants (~9 Hz) confirm ortho

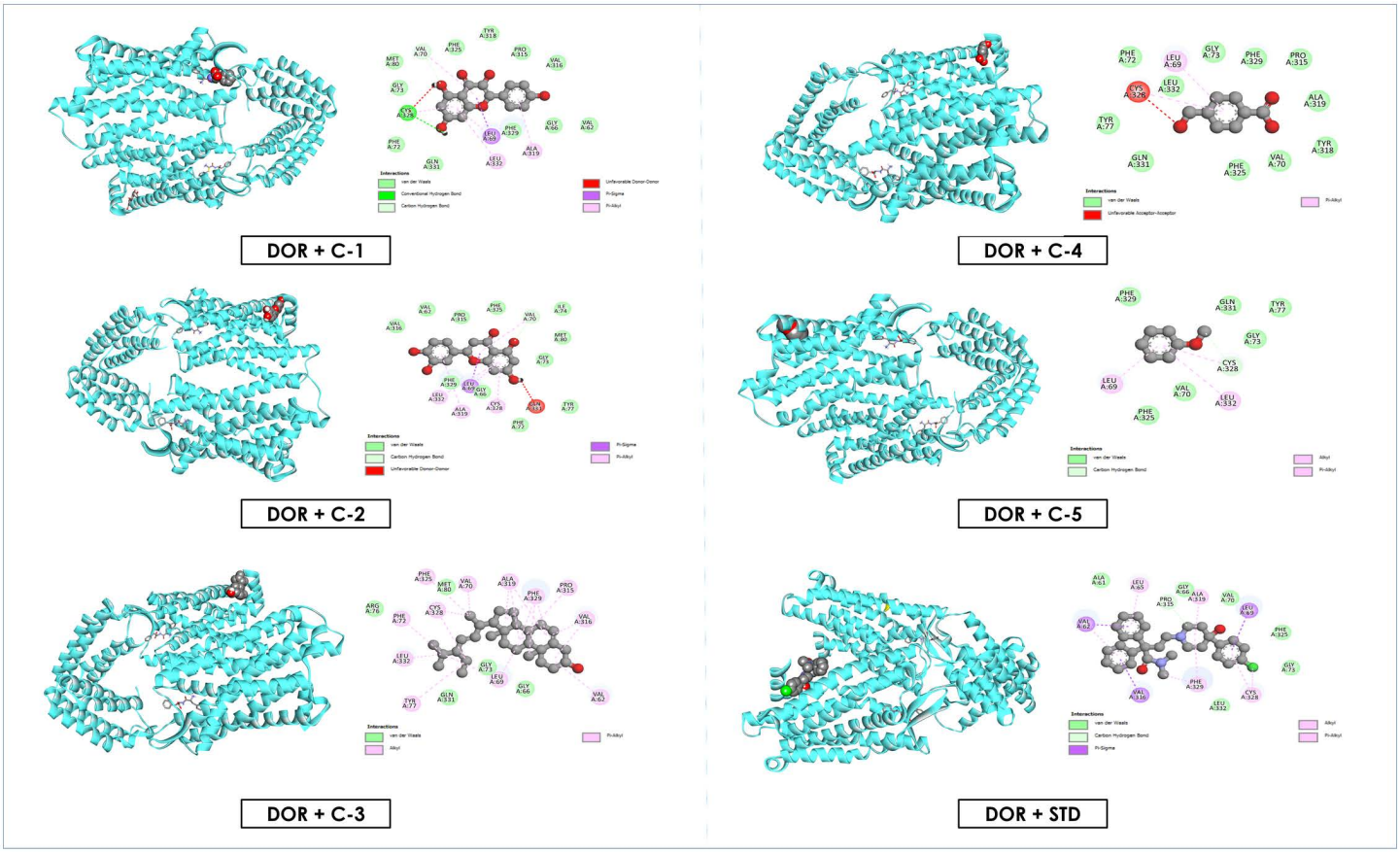


Fig 9. Docking interactions of the isolated compounds with the delta-opioid receptor (DOR). The figure presents three-dimensional ligand binding orientations along with two-dimensional interaction maps, illustrating hydrogen bonding, hydrophobic contacts, and other stabilizing interactions between the ligands and residues within the receptor binding pocket.

https://doi.org/10.1371/journal.pone.0351085.g009

relationships, while the symmetry of the two equivalent sets of protons is consistent with para substitution on the aromatic ring. In addition, a singlet resonance at δ 4.58 ppm integrating for two protons was assigned to the benzylic methylene group (–CH2OH). The absence of splitting in this signal indicates that the two protons are magnetically equivalent, while the deshielding effect of the adjacent aromatic carboxyl group accounts for its chemical shift in the downfield region. Overall, the splitting pattern and chemical shifts are fully consistent with the proposed structure of **4-Carboxybenzyl alcohol**, confirming the presence of a para-substituted benzyl system with both carboxyl and hydroxymethyl functional groups in expected positions.

The 1H NMR spectrum (MeOD-d4, 600 MHz) of **Compound 5** exhibits signals that clearly reflect its symmetrical para-substituted aromatic structure. The doublet at 7.41 ppm (2H, J = 7.2 Hz) is attributed to the aromatic protons located ortho to the methoxy group (positions 2 and 6), while the second doublet at 6.79 ppm (2H, J = 7.8 Hz) corresponds to the protons at positions 3 and 5. These splitting patterns arise due to typical ortho-coupling interactions between adjacent aromatic protons, and the near-equal coupling constants further support the symmetrical nature of the molecule. Additionally, a singlet observed at 3.83 ppm integrating for three protons corresponds to the methoxy group (-OCH3) attached to the para position of the benzene ring. The absence of coupling confirms that the methoxy protons are isolated from other hydrogen interactions. The overall pattern—two doublets for the aromatic protons and a singlet for the methoxy group—is

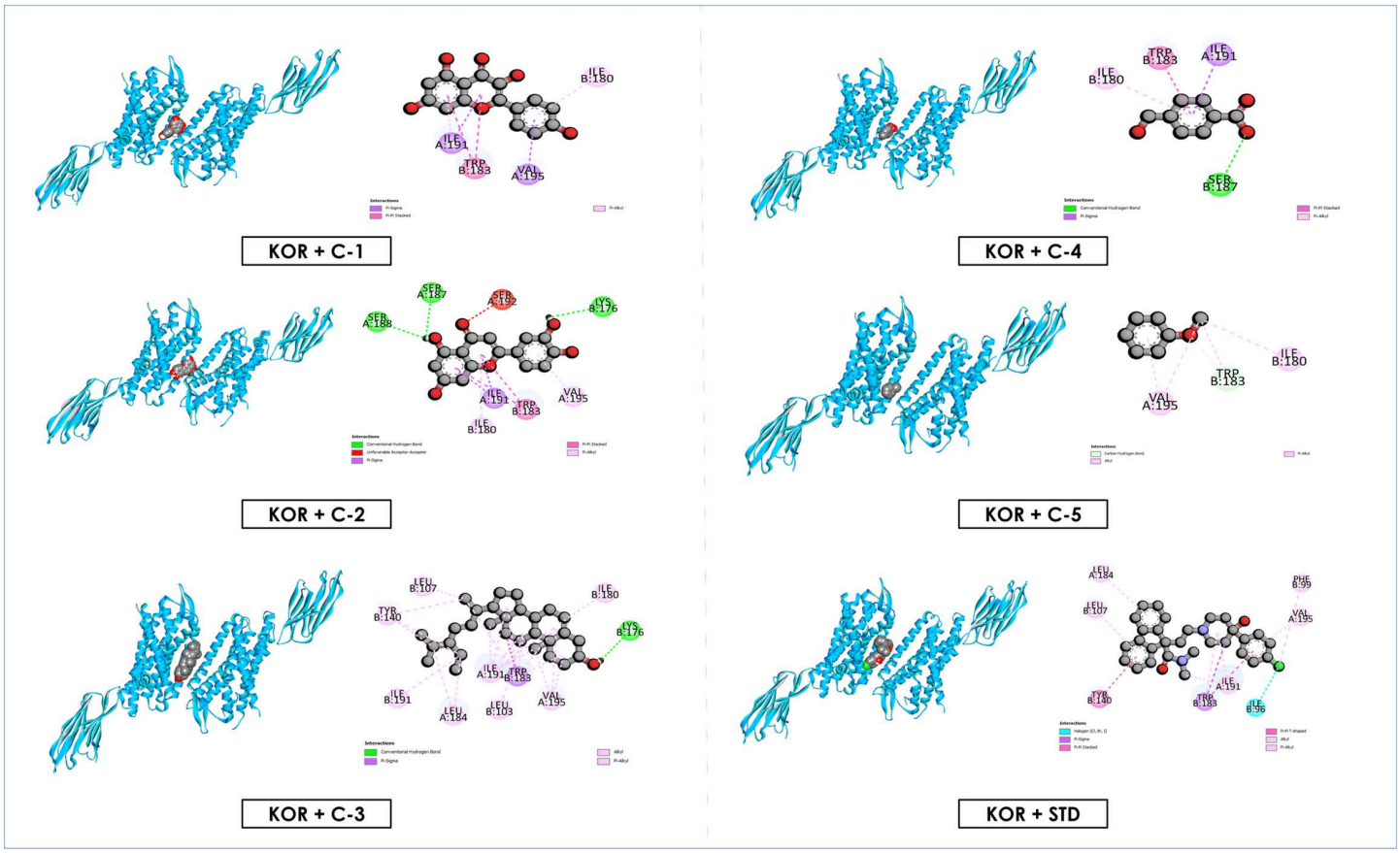


Fig 10. Docking interactions of the isolated compounds with the kappa-opioid receptor (KOR). The 3D binding poses and corresponding 2D interaction diagrams demonstrate the positioning of the ligands within the receptor binding cavity and highlight key amino acid interactions contributing to ligand stabilization, including hydrogen bonding and hydrophobic contacts.

https://doi.org/10.1371/journal.pone.0351085.g010

characteristic of a para-substituted aromatic ether and supports the identity of the compound as **4-methoxybenzaldehyde**. The symmetry simplifies the spectrum, resulting in clearly resolved and easily assignable peaks.

Again the present study establishes the broad pharmacological potential of *Eichhornia crassipes* flower extract (CME), demonstrating significant antidiarrheal, antimicrobial, and thrombolytic activities. The marked dose-dependent suppression of castor oil–induced diarrhea indicates that CME influences intestinal motility and fluid secretion. Phytoconstituents such as flavonoids, tannins, alkaloids, and phenolics are well known for their ability to inhibit prostaglandin synthesis, enhance water and electrolyte reabsorption, and reduce gastrointestinal hyperactivity [40]. Such mechanisms are consistent with the profound effect observed at higher doses, which were comparable to the standard loperamide.

The antimicrobial investigation revealed that the extracts exhibited moderate to significant zones of inhibition (ZOI), which were largely supported by corresponding MIC values, indicating genuine antimicrobial potential. Among the fractions, DSF and CME demonstrated superior activity, evidenced by larger inhibition zones (up to ~20 mm) and lower MIC values (as low as 15.6 µL/mL), particularly against Gram-positive bacteria such as *B. subtilis* and *S. aureus*. This trend aligns with previous studies reporting that moderately non-polar fractions often concentrate bioactive phytoconstituents with strong antimicrobial effects [41,42]. The PSF fraction showed selective moderate activity, with notable effects against *S. typhi* and *S. dysenteriae*, while remaining less active against other strains. This organism-specific behavior may be

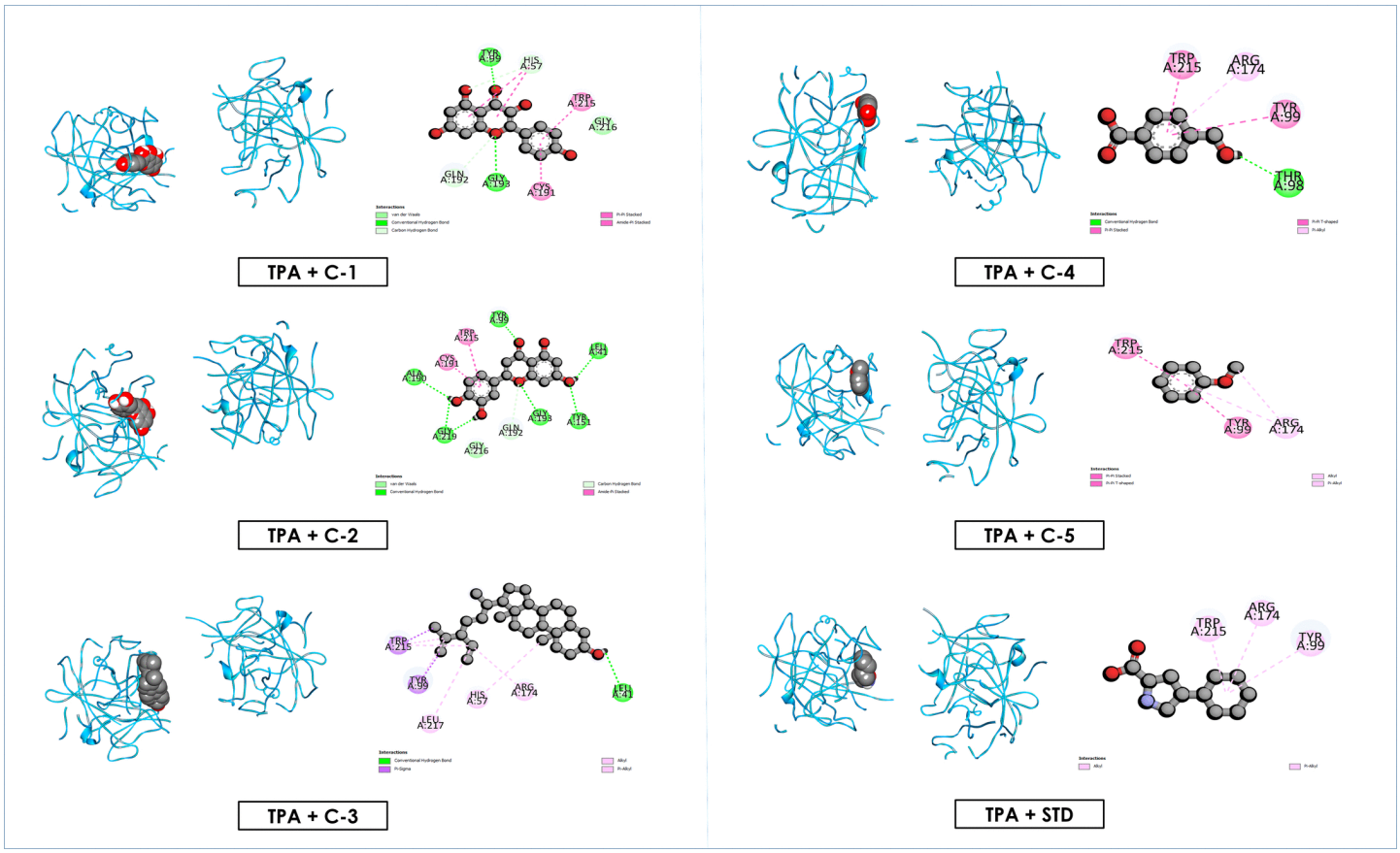


Fig 11. Docking interactions of the isolated compounds with tissue plasminogen activator (TPA). The 3D ligand–receptor complexes and 2D interaction maps depict the binding orientation of the compounds within the TPA active site and illustrate hydrogen bonding and hydrophobic interactions with surrounding residues, which may contribute to the predicted binding affinity.

https://doi.org/10.1371/journal.pone.0351085.g011

attributed to the presence of lipophilic compounds, such as terpenoids and fatty acid derivatives, which can disrupt microbial cell membranes but may have limited diffusion capacity in agar media [43]. Consequently, some discrepancies between ZOI and MIC values were observed, which is common in plant extract studies due to differences in compound diffusion, solubility, and interaction with agar matrices [44].

In general, Gram-positive bacteria were more susceptible than Gram-negative bacteria, as reflected by larger ZOI and lower MIC values. This can be explained by the structural differences in their cell envelopes; Gram-negative bacteria possess an outer membrane rich in lipopolysaccharides that restricts the penetration of many phytochemicals [45]. Additionally, the absence of this outer barrier in Gram-positive bacteria facilitates enhanced interaction of lipophilic and phenolic compounds with the cytoplasmic membrane, leading to increased permeability and cellular leakage [41,46]. The comparatively weaker antifungal activity observed may be due to the rigid chitin-containing cell wall of fungi, which reduces susceptibility to plant-derived compounds [47]. The antimicrobial mechanisms of the active fractions are likely multifactorial, involving cell membrane disruption, protein denaturation, enzyme inhibition, and interference with nucleic acid synthesis, depending on the phytochemical composition. Compounds such as flavonoids, phenolics, and sterols—previously identified in similar plant extracts—are known to exert antimicrobial effects through membrane permeability alteration and oxidative stress induction [48,49].

The antimicrobial effects of the PSF can be further rationalized by the presence of identified compounds such as kaempferol, luteolin, and stigmasterol. Flavonoids like kaempferol and luteolin are reported to exert antimicrobial activity through multiple mechanisms, including inhibition of nucleic acid synthesis, disruption of energy metabolism, and induction of oxidative stress [50,51]. Meanwhile, sterol compounds such as stigmasterol may contribute to membrane destabilization due to their lipophilic nature, potentially altering membrane fluidity and integrity. These findings suggest a multifactorial and potentially synergistic mode of action within the crude fraction. Overall, the findings suggest that solvent polarity plays a critical role in extracting bioactive compounds, with DSF and CME being the most effective fractions. The observed variation between ZOI and MIC further emphasizes the importance of combining diffusion-based and dilution-based assays to accurately evaluate antimicrobial potential.

The thrombolytic assay revealed that the extracts of *E. crassipes* flowers possess measurable clot-dissolving activity *in vitro*. Although the observed activity was lower than that of the standard SK, the results indicate the presence of phytochemicals capable of influencing fibrinolytic processes. Previous studies have suggested that polyphenolic compounds, particularly flavonoids and tannins, may contribute to thrombolytic effects through mechanisms such as plasminogen activation, fibrin degradation, or inhibition of platelet aggregation [52]. The presence of such phytochemicals in *E. crassipes* flowers may therefore account for the clot lysis activity observed in this study. Although certain fractions exhibited comparatively higher thrombolytic activity, the PSF fraction was selected for phytochemical investigation because it yielded isolable compounds in sufficient quantities for structural characterization and subsequent molecular docking and ADMET analysis. This fraction enabled the identification of stigmasterol, kaempferol, and luteolin, which were further evaluated to explore their possible interactions with relevant biological targets. These findings provide preliminary insight into the potential role of these phytochemicals in the observed biological activity and support further investigation of *E. crassipes* flowers as a source of pharmacologically relevant compounds.

The docking outcomes suggest that Stigmasterol, Luteolin, and Kaempferol may contribute to the pharmacological activities observed in the PSF of *E. crassipes*. Stigmasterol, in particular, showed the strongest predicted binding affinity for the kappa opioid receptor (–10.3 kcal/mol), indicating a possible interaction with opioid-mediated pathways involved in intestinal motility and thereby providing a hypothetical mechanistic explanation for the antidiarrheal activity observed in experimental assays. Luteolin also displayed notable predicted interactions with both delta- and kappa-opioid receptors (–8.1 and –9.1 kcal/mol), which is consistent with previous reports suggesting that certain flavonoids may influence opioid and prostaglandin signaling pathways involved in gastrointestinal regulation (**Table 5**, **Figs 9 and 10**) [53].

The antimicrobial docking profiles of these flavonoids (Luteolin and Kaempferol) and sterols (Stigmasterol) indicated moderate predicted binding interactions (–7.5 to –8.4 kcal/mol) with antimicrobial targets. While these findings provide supportive computational evidence, they should not be interpreted as definitive proof of bacteriostatic activity, and experimental validation through enzyme inhibition or mechanistic assays would be required. Nevertheless, these predicted interactions align with previous reports describing how polyphenolic and sterol-based metabolites may disrupt bacterial membranes or interfere with folate metabolism and nucleic acid synthesis (**Table 5**, **Figs 7 and 8**) [41,54].

Similarly, docking against the thrombolytic target suggested that Stigmasterol, Luteolin, and Kaempferol may interact with the tissue plasminogen activator (TPA) binding site, with predicted affinities ranging from –7.6 to –8.0 kcal/mol (**Table 5**, **Fig 11**). Although these values were higher than the calculated score for streptokinase in this docking model, such comparisons should be interpreted cautiously because computational docking scores do not necessarily translate directly into biological potency. These findings therefore provide preliminary hypotheses that may help explain the moderate *in vitro* clot-lysis activity observed and warrant further biochemical investigation [23]. It is important to note that docking scores reflect binding propensity rather than pharmacological efficacy and should therefore be interpreted as hypothesis-generating rather than confirmatory evidence.

The pharmacokinetic characteristics of the isolated phytochemicals were further explored through in silico ADMET analysis, which provides preliminary insights into the absorption, distribution, metabolism, excretion, and toxicity profiles of

candidate molecules during early drug discovery. The predicted absorption parameters indicated generally favorable oral bioavailability for most compounds. Kaempferol and Luteolin demonstrated moderate aqueous solubility and good predicted intestinal absorption (>74–81%), whereas Stigmasterol showed lower solubility due to its highly lipophilic steroidal structure (**Table 6**). This elevated lipophilicity (high LogP) is known to reduce aqueous solubility and may adversely affect oral bioavailability despite favorable membrane permeability, a common limitation observed in sterol-type compounds [55,56]. Such reduced solubility is a common limitation of sterol-type molecules and may influence their oral bioavailability despite good membrane permeability. The Caco-2 permeability predictions suggested that several of the investigated compounds are capable of crossing intestinal epithelial barriers, while the predicted P-glycoprotein interactions indicate that flavonoids such as Kaempferol and Luteolin may be subjected to efflux transport mechanisms that could influence their intracellular concentration. Similar transport interactions have been widely reported for polyphenolic compounds during pharmacokinetic evaluation [57,58].

Distribution and metabolic predictions provided additional insights into the systemic behavior of the identified phytochemicals. Kaempferol and Luteolin displayed moderate predicted volumes of distribution and limited blood–brain barrier permeability, suggesting that their pharmacological effects are more likely to occur through systemic circulation rather than central nervous system interactions. Conversely, Stigmasterol showed higher predicted lipophilicity and potential blood–brain barrier penetration, which may influence tissue distribution patterns. Cytochrome P450 metabolism predictions indicated that most of the compounds are not substrates of CYP2D6, while Stigmasterol may undergo metabolism through CYP3A4, the major enzyme involved in xenobiotic metabolism [59]. Toxicity prediction models suggested generally favorable safety profiles, with no predicted AMES mutagenicity or hepatotoxicity for the evaluated molecules, although a possible hERG II inhibition signal for Stigmasterol indicates that further experimental safety evaluation would be necessary [56]. Drug-likeness analysis based on Lipinski's rule of five demonstrated that Kaempferol and Luteolin satisfy the criteria commonly associated with orally active compounds, whereas Stigmasterol showed a single violation due to high lipophilicity, a characteristic frequently observed among steroid-like natural products [57]. Such high lipophilicity may also result in poor dissolution rate and variable absorption, necessitating formulation strategies to enhance its pharmacokinetic performance [56].

The bioavailability radar plot (**Fig 12**) further illustrated the physicochemical drug-likeness of the identified compounds by integrating key parameters such as lipophilicity, polarity, molecular size, solubility, flexibility, and saturation. Kaempferol and Luteolin were largely positioned within the optimal physicochemical region predicted by the radar model, indicating balanced drug-like properties [60]. In contrast, Stigmasterol showed deviations primarily related to excessive lipophilicity and reduced polarity, which may contribute to its limited aqueous solubility. Complementary evaluation using the BOILED-Egg model (**Fig 13**) provided additional insight into gastrointestinal absorption and blood–brain barrier permeability. In this model, Kaempferol and Luteolin were predicted to lie within the white region associated with a high probability of passive gastrointestinal absorption while remaining outside the yellow "yolk" region representing brain penetration. This pattern suggests that these flavonoids may exert pharmacological effects primarily through systemic exposure rather than central nervous system activity. Collectively, the ADMET predictions indicate that Kaempferol and Luteolin possess relatively balanced pharmacokinetic characteristics, whereas Stigmasterol may require formulation optimization to overcome solubility limitations. Nevertheless, these computational predictions remain preliminary and should be interpreted cautiously until confirmed through experimental pharmacokinetic and toxicological investigations [56,60].

Altogether, stigmasterol, luteolin, and kaempferol may represent potential multitarget phytochemicals capable of contributing to the management of diarrhea, microbial infections, and thrombotic complications. The molecular docking results, together with favorable pharmacokinetic predictions, suggest possible interactions with relevant biological targets, indicating their promise as polypharmacological leads. However, these computational findings should be interpreted cautiously, as docking simulations provide predictive insights rather than definitive evidence of biological activity. Although the calculated binding affinities were comparable to those of standard ligands such as ciprofloxacin, loperamide, and

Table 6. ADME/T of isolated compounds from PSF of methanolic extract of flower of *E. crassipes*.

Properties	Model name (Unit)	Kaempferol	Luteolin	Stigmasterol	4-Carboxybenzyl alcohol	4-Methoxy benzene
Absorption	Water solubility (log mol/L)	−3.04	−3.094	−6.682	−1.931	−1.608
	Caco2 permeability (log Papp in 10−6 cm/s)	0.032	0.096	1.213	1.092	1.529
	Intestinal absorption (human) (% Absorbed)	74.29	81.13	94.97	82.432	96.278
	Skin Permeability (log Kp)	−2.735	−2.735	−2.783	−2.734	−1.814
	P-glycoprotein substrate	Yes	Yes	No	No	No
	P-glycoprotein I inhibitor	No	No	Yes	No	No
	P-glycoprotein II inhibitor	No	No	Yes	No	No
Distribution	VDss (human) (log L/kg)	1.274	1.153	0.178	−1.572	0.106
	Fraction unbound (human) (Fu)	0.178	0.168	0	0.67	0.387
	BBB permeability	−0.939	−0.907	0.771	−0.316	0.47
	CNS permeability	−2.228	−2.251	−1.652	−2.871	−1.791
Metabolism	CYP2D6 substrate	No	No	No	No	No
	CYP3A4 substrate	No	No	Yes	No	No
	CYP1A2 inhibitior	Yes	Yes	No	No	No
	CYP2C19 inhibitior	No	No	No	No	No
	CYP2C9 inhibitior	No	Yes	No	No	No
	CYP2D6 inhibitior	No	No	No	No	No
	CYP3A4 inhibitor	No	No	No	No	No
Excretion	Total Clearance (log mL/min/kg)	0.477	0.495	0.618	0.276	0.271
	Renal OCT2 substrate	No	No	No	No	No
Toxicity	AMES toxicity	No	No	No	No	No
	Max. tolerated dose (human) (log mg/kg/day)	0.531	0.499	−0.664	1.534	1.173
	hERG I inhibitor	No	No	No	No	No
	hERG II inhibitor	No	No	Yes	No	No
	Oral Rat Acute Toxicity (LD50) (mol/kg)	2.449	2.455	2.54	1.871	1.915
	Oral Rat Chronic Toxicity (LOAEL) (log mg/kg_bw/day)	2.505	2.409	0.872	2.745	1.964
	Hepatotoxicity	No	No	No	No	No
	Skin Sensitisation	No	No	No	No	Yes
	T.Pyriformis toxicity (log ug/L)	0.312	0.326	0.433	0.231	−0.119
	Minnow toxicity (log mM)	2.885	3.169	−1.675	2.548	1.51
	Molecular weight (g/mol)	286.24	286.24	412.69	151.14	108.14
Drug-likeness	Num. H-bond acceptors	6	6	1	3	1
	Num. H-bond donors	4	4	1	1	0
	topological polar surface area (TPSA) (Å²)	111.13	111.13	20.23	60.36	9.23
	Consensus Log Po/w	1.58	1.73	6.98	0.74	1.88
	Lipinski's RO5 violation	Yes; 0 violation	Yes; 0 violation	Yes; 1 violation: MLOGP>4.15	Yes; 0 violation	Yes; 0 violation
	Bioavailability Score (%)	0.55	0.55	0.55	0.85	0.55

https://doi.org/10.1371/journal.pone.0351085.t006

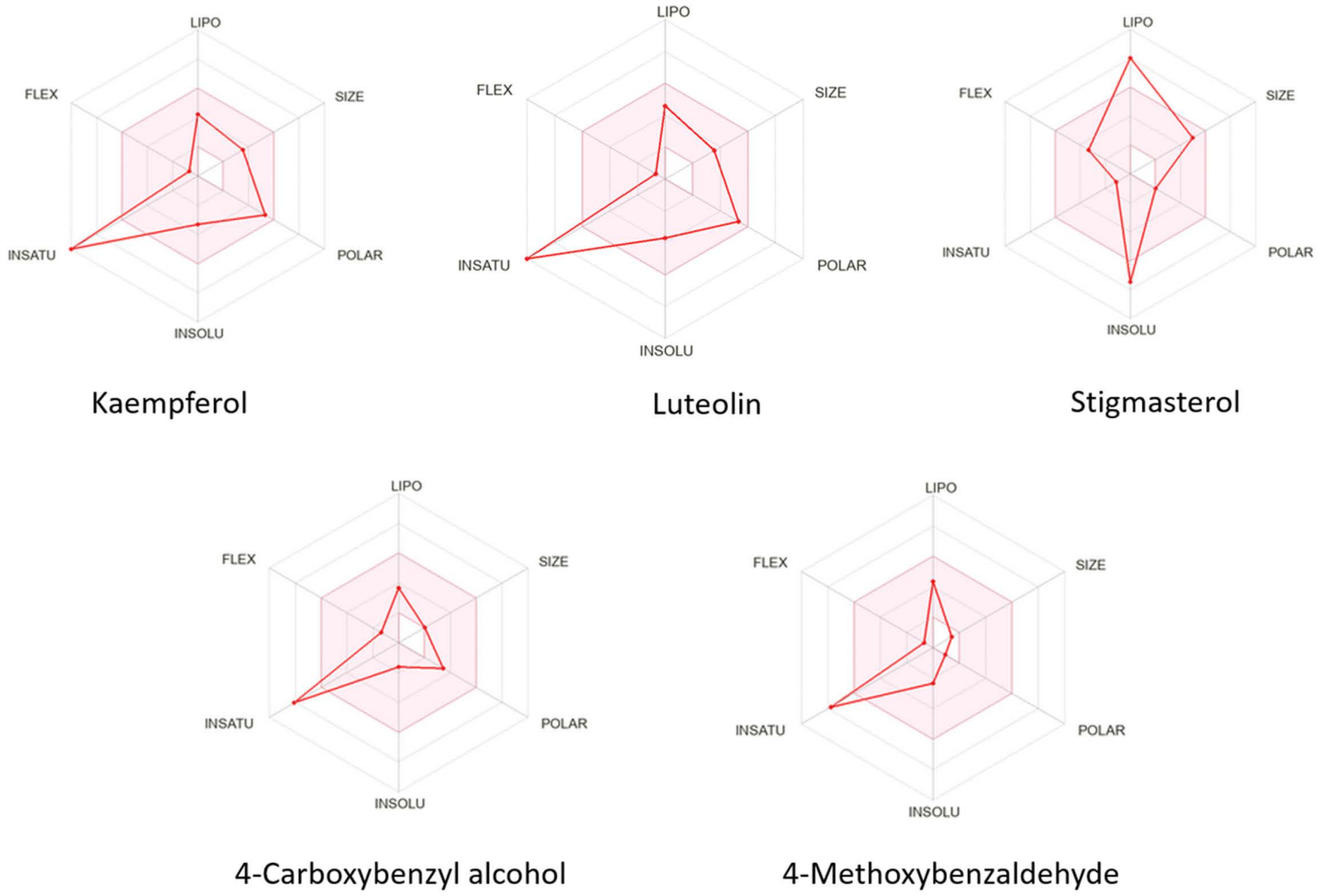


Fig 12. Radar images of isolated from PSF of methanolic extract of flower of *E. crassipes*.

https://doi.org/10.1371/journal.pone.0351085.g012

streptokinase in some cases, experimental validation is necessary to confirm these interactions and their pharmacological relevance. Furthermore, limitations such as poor aqueous solubility and potential efflux susceptibility—common characteristics of many polyphenolic compounds—highlight the need for formulation optimization and improved delivery strategies. Future studies involving bioassay-guided fractionation, target-specific biochemical assays, and expanded in vivo investigations will be essential to clarify the therapeutic potential of these phytoconstituents and to translate the present in silico predictions into practical pharmacological applications.

Limitations and future prospective

Although this study provides compelling evidence of the pharmacological potential of the petroleum ether soluble fraction of *Eichhornia crassipes* flowers, several limitations need to be considered before translating these findings into clinical applications. The antimicrobial and thrombolytic activities observed were moderate compared to conventional drugs, which reduces their immediate therapeutic applicability. MIC values were determined to strengthen antimicrobial evaluation; however, additional studies such as minimum bactericidal concentration (MBC), time–kill kinetics, and pathogen-specific infection models (including diarrhea-relevant strains such as *Escherichia coli*) would provide a more

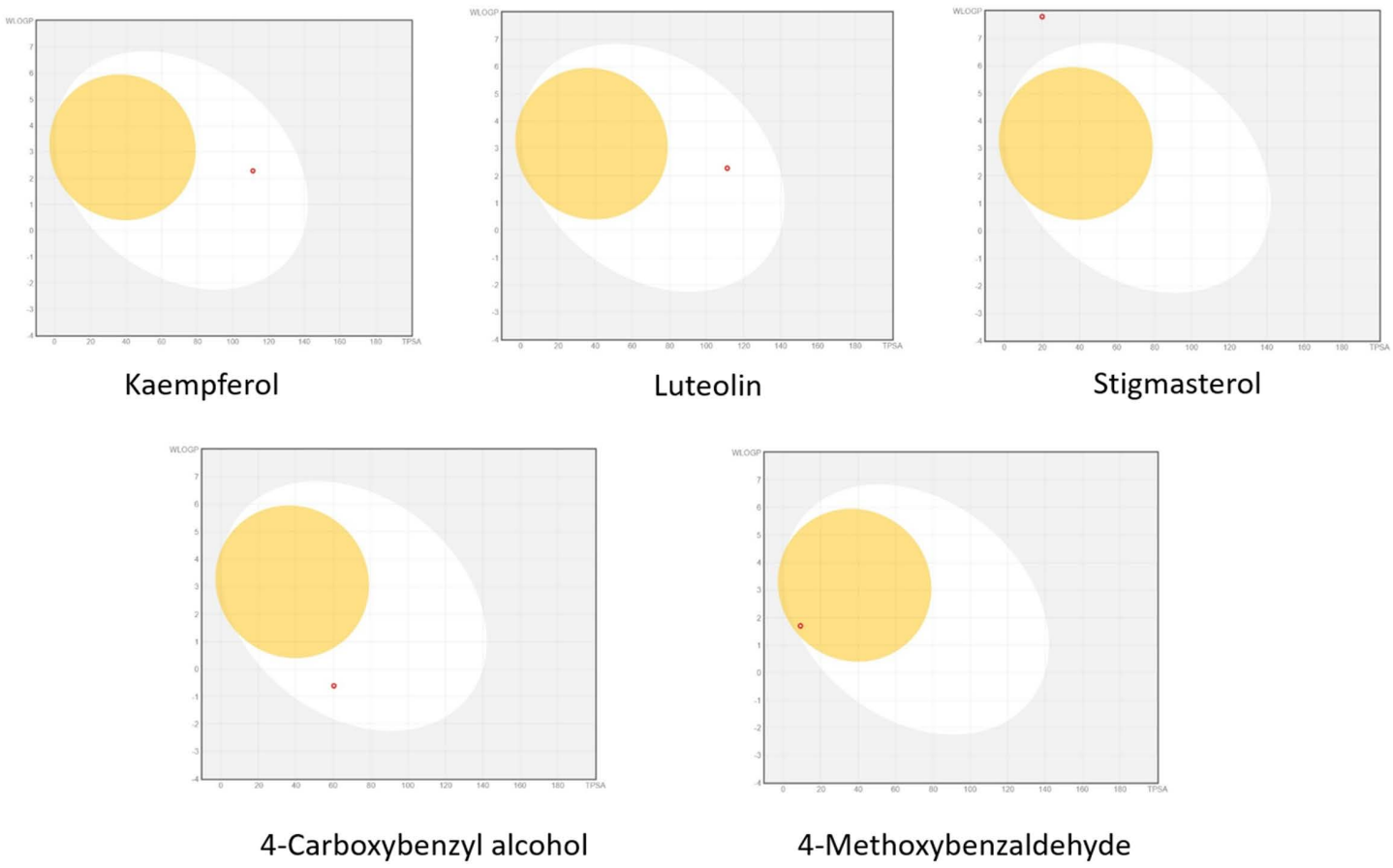


Fig 13. Boiled egg images of isolated from PSF of methanolic extract of flower of *E. crassipes*.

https://doi.org/10.1371/journal.pone.0351085.g013

comprehensive assessment. The *in vivo* experiments were conducted using relatively small animal groups (n = 4 per group), consistent with preliminary pharmacological screening and ethical principles of animal use (Reduction). However, this sample size may increase the risk of Type II error. Although the observed dose-dependent reductions in diarrheal count and the magnitude of differences between treated and control groups suggest a substantial biological effect, future studies incorporating a priori power analysis (e.g., using G*Power), larger cohorts, and additional endpoints such as latent period, intestinal transit, and enteropooling assays are necessary to strengthen statistical robustness and translational relevance.

Furthermore, while the study successfully isolated five compounds, it did not employ bioassay-guided fractionation, which could have provided a clearer understanding of which specific phytochemicals were responsible for the observed biological activities. In addition, although the isolated compounds were characterized using ^{1}H NMR spectroscopy and comparison with published data, more comprehensive structural elucidation techniques (e.g., ^{13}C NMR, HMBC, HSQC, or HRMS) and quantitative purity assessment (e.g., HPLC-DAD profiling) were not included, as the present study was primarily designed as an exploratory phytochemical and pharmacological investigation focused on compound isolation and preliminary activity evaluation. In addition, the limited yield of certain isolates constrained extensive analytical characterization without compromising sample availability.

Another limitation lies in the reliance on in silico docking and ADMET predictions, which, though valuable, remain predictive tools and cannot replace detailed pharmacokinetic and pharmacodynamic evaluations in living systems. Additionally, no advanced toxicological assessment or evaluation of human clinical relevance was performed, which limits direct translational applicability of the findings. Moreover, stigmasterol, despite its strong docking performance and promising activity, demonstrated physicochemical drawbacks such as high lipophilicity and low aqueous solubility, which may limit its bioavailability and restrict its practical therapeutic use without further formulation improvements.

Looking forward, future research should address these limitations through more targeted experimental approaches. Bioassay-guided fractionation combined with advanced analytical techniques would allow clearer identification of the specific compounds responsible for the observed activities. Comprehensive metabolite profiling using chromatographic techniques such as HPLC-DAD or LC–MS is also warranted to quantify relative abundance and confirm purity of the isolated constituents. In addition, mechanistic validation studies, including enzyme inhibition assays, receptor-binding experiments, and disease-relevant animal models, are necessary to confirm the biological targets suggested by docking analyses. Expanding in vivo investigations with larger animal cohorts and improved statistical power would also strengthen the reliability of pharmacological findings. Additionally, incorporation of adequately powered study designs and refined pharmacological endpoints will enhance the robustness of future evaluations. Given the physicochemical limitations observed for some compounds, particularly stigmasterol, formulation strategies such as nanoemulsions, liposomal delivery systems, or other nanocarrier-based approaches may improve solubility and bioavailability. Furthermore, synergy studies with conventional antimicrobial, antidiarrheal, or thrombolytic agents may reveal additive or potentiating effects that could enhance therapeutic relevance. Finally, comprehensive preclinical evaluations including pharmacokinetics, toxicity profiling, and long-term safety studies will be essential to determine whether these phytochemicals can be translated into viable therapeutic candidates.

Conclusion

The present study demonstrates that the petroleum ether soluble fraction of *Eichhornia crassipes* flowers contains bioactive phytochemicals with diverse pharmacological potential. Phytochemical isolation led to the identification of stigmasterol, kaempferol, and luteolin, which may contribute to the biological activities observed in the experimental assays. The extract exhibited dose-dependent antidiarrheal activity *in vivo*, along with moderate antimicrobial activity against several bacterial and fungal pathogens and measurable thrombolytic activity *in vitro*. Although the thrombolytic effect was lower than that of the reference drug streptokinase, the results indicate a multifaceted pharmacological profile for this plant fraction. Complementary molecular docking analyses provided predictive insights into possible ligand–target interactions, suggesting that the identified phytochemicals may interact with proteins associated with antimicrobial, antidiarrheal, and thrombolytic pathways, including DHFR, KAS, opioid receptors, and tissue plasminogen activator. These findings highlight *E. crassipes* flowers as a potential source of multifunctional phytochemicals that may contribute to the development of plant-derived therapeutic leads. However, further studies involving bioassay-guided fractionation, mechanistic validation, pharmacokinetic evaluation, and advanced in vivo models will be necessary to fully establish the therapeutic relevance of these compounds. Overall, this study provides new insights into the pharmacological value of *E. crassipes* and supports continued exploration of this widely available aquatic plant as a potential resource for drug discovery.

Supporting information

S1 File. Meta data of *In vitro* and *In vivo* experiments.
(XLSX)

S2 File. Meta data of molecular docking.
(RAR)

S3 File. Figure: Graphical Abstract.
(TIF)

Author contributions

Conceptualization: Md. Mirazul Islam, Suriya Akter Shompa, Hasin Hasnat, Safaet Alam, Mohammad A. Rashid.

Data curation: Md. Mirazul Islam, Suriya Akter Shompa, Hasin Hasnat, Safaet Alam, Md. Sakhawat Hossain.

Formal analysis: Suriya Akter Shompa, Hasin Hasnat, Saima Jahan Riti, Ferdousy Kabir, Md. Sakhawat Hossain.

Funding acquisition: Mohammad A. Rashid.

Investigation: Md. Mirazul Islam, Suriya Akter Shompa, Hasin Hasnat, Safaet Alam, Saima Jahan Riti, Ferdousy Kabir.

Methodology: Md. Mirazul Islam, Suriya Akter Shompa, Hasin Hasnat, Safaet Alam, Saima Jahan Riti, Mohammad A. Rashid.

Project administration: Md. Mirazul Islam, Hasin Hasnat, Safaet Alam, Mohammad A. Rashid.

Resources: Md. Mirazul Islam, Hasin Hasnat, Safaet Alam, Mohammad A. Rashid.

Software: Md. Mirazul Islam, Suriya Akter Shompa, Hasin Hasnat, Safaet Alam, Ferdousy Kabir, Md. Sakhawat Hossain.

Supervision: Md. Mirazul Islam, Safaet Alam, Mohammad A. Rashid.

Validation: Md. Mirazul Islam, Suriya Akter Shompa, Hasin Hasnat, Safaet Alam, Ferdousy Kabir, Md. Sakhawat Hossain, Mohammad A. Rashid.

Visualization: Md. Mirazul Islam, Hasin Hasnat, Safaet Alam, Md. Sakhawat Hossain, Mohammad A. Rashid.

Writing – original draft: Md. Mirazul Islam, Suriya Akter Shompa, Hasin Hasnat, Safaet Alam.

Writing – review & editing: Md. Mirazul Islam, Hasin Hasnat, Safaet Alam, Saima Jahan Riti, Ferdousy Kabir, Md. Sakhawat Hossain, Mohammad A. Rashid.

References

1. Taher MA, Hasnat H, Alam S, Akter S, Afroze M, Khan M. Indian Shot (Canna Indica L). leaves provide valuable insights into the management of inflammation and other associated disorders offering health benefits. J Inflamm Res. 2024;:10943–89.
2. Hasnat H, Riti J, Shompa A, Alam S, Islam MM, Kabir F. Unveiling the therapeutic potentials of water hyacinth (Eichhornia crassipes (Mart.) Solms) flower against oxidative stress, inflammation and depressive disorders: GC-MS/ MS, in vitro, in vivo and in silico approaches. Chem Biodivers. 2024;202401268(12):e202401268. https://doi.org/10.1002/cbdv.202401268
3. Hasnat H, Alam S, Akter Shompa S, Saha T, Richi FT, Hossain MH, et al. Phyto-pharmacological wonders of genus Ficus: ethnopharmacological insights and phytochemical treasures from natural products. Saudi Pharm J. 2024;32(12):102211. https://doi.org/10.1016/j.jsps.2024.102211 PMID: 39697478
4. Alam S, Richi FT, Hasnat H, Ahmed F, Emon NU, Uddin MJ, et al. Chemico-pharmacological evaluations of the dwarf elephant ear (Colocasia affinis Schott) plant metabolites and extracts: health benefits from vegetable source. Front Pharmacol. 2024;15:1428341. https://doi.org/10.3389/fphar.2024.1428341 PMID: 39193333
5. Taher MA, Islam MA, Tasmi SF, Hasan MM, Hasnat H, Shompa SA, et al. Phytochemical profiling and bioactivity validation of Moringa oleifera leaves: antimicrobial, antidiarrheal, analgesic, and in silico insights. PLoS One. 2025;20(9):e0332048. https://doi.org/10.1371/journal.pone.0332048 PMID: 40938821
6. Mujere N. Water hyacinth: characteristics, problems, control options, and beneficial uses. Impact Water Pollut Hum Heal Environ Sustain. 2016:343–61.
7. Dymond EA. The water hyacinth (Eichhornia crassipes), a Cinderella of plant world and its uses. J Aquat Work. 2002;2:205–10.
8. Sharma AK, Sharma V, Sharma V, Sharma JK, Singh R. Multifaceted potential of Eichhornia crassipes (Water Hyacinth) ladened with numerous value aided and therapeutic properties. Plant Arch. 2020;20(2):2059–65.
9. Dineshkumar G, Rajakumar R, Mani P, Johnbastin TMM. Hepatoprotective activity of leaves extract of Eichhornia crassipes against CCl4 induced hepatotoxicity albino rats. Int J Pure Appl Zool. 2013;1(3):209–12.

10. Aboul-Enein AM, Shanab SMM, Shalaby EA, Zahran MM, Lightfoot DA, El-Shemy HA. Cytotoxic and antioxidant properties of active principals isolated from water hyacinth against four cancer cells lines. BMC Complement Altern Med. 2014;14:397. https://doi.org/10.1186/1472-6882-14-397 PMID: 25315352
11. GBD 2021 Diseases and Injuries Collaborators. Global burden of 371 diseases and injuries in 204 countries and territories, 1990–2021: a systematic analysis for the Global Burden of Disease Study 2021. Lancet. 2024;403(10440):2100–32.
12. GBD 2016 Diarrhoeal Disease Collaborators. Estimates of the global, regional, and national morbidity, mortality, and aetiologies of diarrhoea in 195 countries: a systematic analysis for the Global Burden of Disease Study 2016. Lancet Infect Dis. 2018;18(11):1211–28. https://doi.org/10.1016/S1473-3099(18)30362-1 PMID: 30243583
13. GBD Diarrhoeal Diseases Collaborators. Estimates of global, regional, and national morbidity, mortality, and aetiologies of diarrhoeal diseases: a systematic analysis for the Global Burden of Disease Study 2015. Lancet Infect Dis. 2017;17(9):909–48. https://doi.org/10.1016/S1473-3099(17)30276-1 PMID: 28579426
14. Collaborators GBDDD. Global burden of diarrhoeal diseases and risk factors, 1990–2019: a systematic analysis for the Global Burden of Disease Study 2019. Lancet Infect Dis. 2020;20(9):1160–72.
15. O'Neill J. Tackling drug-resistant infections globally: final report and recommendations. London: Review on Antimicrobial Resistance; 2016.
16. Hasnat H, Shompa SA, Islam MM, Alam S, Richi FT, Emon NU, et al. Flavonoids: a treasure house of prospective pharmacological potentials. Heliyon. 2024;10(6):e27533. https://doi.org/10.1016/j.heliyon.2024.e27533 PMID: 38496846
17. VanWagenen BC, Larsen R, Cardellina JH, Randazzo D, Lidert ZC, Swithenbank C. Ulosantoin, a potent insecticide from the sponge Ulosa ruetzleri. J Organ Chem. 1993;58(2):335–7.
18. Ashrafi S, Alam S, Islam A, Emon NU, Islam QS, Ahsan M. Chemico-biological profiling of Blumealacera (Burm. f.) DC. (Family: Asteraceae) provides new insights as a potential source of antioxidant, cytotoxic, antimicrobial, and antidiarrheal agents. Evid-Based Complement Altern Med. 2022;2022(1):2293415. https://doi.org/10.1155/2022/2293415
19. Huys G, D'Haene K, Swings J. Influence of the culture medium on antibiotic susceptibility testing of food-associated lactic acid bacteria with the agar overlay disc diffusion method. Lett Appl Microbiol. 2002;34(6):402–6. https://doi.org/10.1046/j.1472-765x.2002.01109.x PMID: 12028419
20. Alam S, Rashid MA, Sarker MMR, Emon NU, Arman M, Mohamed IN, et al. Antidiarrheal, antimicrobial and antioxidant potentials of methanol extract of Colocasia gigantea Hook. f. leaves: evidenced from in vivo and in vitro studies along with computer-aided approaches. BMC Complement Med Ther. 2021;21(1):119. https://doi.org/10.1186/s12906-021-03290-6 PMID: 33845836
21. Yeasmin MstS, Uddin MdJ, Dey SS, Barmon J, Ema NT, Rana GMM, et al. Optimization of green microwave-assisted extraction of essential oil from lemon (Citrus limon) leaves: Bioactive, antioxidant and antimicrobial potential. Curr Res Green Sustain Chem. 2024;8:100413. https://doi.org/10.1016/j.crgsc.2024.100413
22. Wu P-P, He H, Hong WD, Wu T-R, Huang G-Y, Zhong Y-Y, et al. The biological evaluation of fusidic acid and its hydrogenation derivative as antimicrobial and anti-inflammatory agents. Infect Drug Resist. 2018;11:1945–57. https://doi.org/10.2147/IDR.S176390 PMID: 30498366
23. Prasad S, Kashyap RS, Deopujari JY, Purohit HJ, Taori GM, Daginawala HF. Development of an in vitro model to study clot lysis activity of thrombolytic drugs. Thromb J. 2006;4:14. https://doi.org/10.1186/1477-9560-4-14 PMID: 16968529
24. Zimmermann M. Ethical guidelines for investigations of experimental pain in conscious animals. Pain. 1983;16(2):109–10. https://doi.org/10.1016/0304-3959(83)90201-4 PMID: 6877845
25. Davis JA. Mouse and rat anesthesia and analgesia. Curr Protoc Neurosci. 2008;(SUPPL. 42):1–21. https://doi.org/10.1002/0471142301.nsa04bs42 PMID: 18428669
26. Shoba FG, Thomas M. Study of antidiarrhoeal activity of four medicinal plants in castor-oil induced diarrhoea. J Ethnopharmacol. 2001;76(1):73–6. https://doi.org/10.1016/s0378-8741(00)00379-2 PMID: 11378284
27. Hasnat H, Shompa SA, Richi FT, Islam MM, Suman MH, Ahmed NU, et al. Bioactive secondary metabolites to combat diabetic complications: evidenced from in silico study. Bangla Pharma J. 2023;26(2):167–84. https://doi.org/10.3329/bpj.v26i2.67807
28. Shahriar S, Shermin SA, Hasnat H, Hossain F, Han A, Geng P. Chemico-pharmacological evaluation of the methanolic leaf extract of Catharanthus ovalis: GC--MS/MS, in vivo, in vitro, and in silico approaches. Front Pharmacol. 2024;15.
29. Shompa SA, Hasnat H, Riti SJ, Islam MM, Alam S, Shao C. Phyto-pharmacological evaluation and characterization of the methanolic extract of the Baccaurea motleyana Müll. Arg seed: Promis insights into its Ther uses. Front Pharmacol. 2024;15.
30. Che T, English J, Krumm BE, Kim K, Pardon E, Olsen RHJ, et al. Nanobody-enabled monitoring of kappa opioid receptor states. Nat Commun. 2020;11(1):1145. https://doi.org/10.1038/s41467-020-14889-7 PMID: 32123179
31. Fenalti G, Zatsepin NA, Betti C, Giguere P, Han GW, Ishchenko A, et al. Structural basis for bifunctional peptide recognition at human δ-opioid receptor. Nat Struct Mol Biol. 2015;22(3):265–8. https://doi.org/10.1038/nsmb.2965 PMID: 25686086
32. Qiu X, Janson CA, Smith WW, Head M, Lonsdale J, Konstantinidis AK. Refined structures of beta-ketoacyl-acyl carrier protein synthase III. J Mol Biol. 2001;307(1):341–56. https://doi.org/10.1006/jmbi.2000.4457 PMID: 11243824
33. Khatun MCS, Muhit MA, Hossain MJ, Al-Mansur MA, Rahman SMA. Isolation of phytochemical constituents from Stevia rebaudiana (Bert.) and evaluation of their anticancer, antimicrobial and antioxidant properties via in vitro and in silico approaches. Heliyon. 2021;7(12):e08475. https://doi.org/10.1016/j.heliyon.2021.e08475 PMID: 34917793

34. Riti SJ, Shompa SA, Hasnat H, Islam MM, Alam S, Ghosh S, et al. The miraculous Asian Fruit Baccaurea motleyana Müll. Arg. (Rambai): exploring the phyto-pharmacological potentials of fruit peel through GC-MS/MS, in vitro, in vivo, and in silico approaches. Chem Biodivers. 2025;22(5):e202402444. https://doi.org/10.1002/cbdv.202402444 PMID: 39663189
35. Ren G, Hou J, Fang Q, Sun H, Liu X, Zhang L, et al. Synthesis of flavonol 3-O-glycoside by UGT78D1. Glycoconj J. 2012;29(5–6):425–32. https://doi.org/10.1007/s10719-012-9410-5 PMID: 22767031
36. Lin L-C, Pai Y-F, Tsai T-H. Isolation of Luteolin and Luteolin-7-O-glucoside from Dendranthema morifolium Ramat Tzvel and Their Pharmacokinetics in Rats. J Agric Food Chem. 2015;63(35):7700–6. https://doi.org/10.1021/jf505848z PMID: 25625345
37. Muharni M, Ferlinahayati F, Yohandini H, Riyanti F, Pakpahan NAP. The anticholesterol activity of betulinic acid and stigmasterol isolated from the leaves of sungkai (Paronema canescens Jack). Int J Appl Pharm. 2021;13(2):198–203.
38. Yang Z, Zhu Z, Luo R, Qiu X, Liu J, Yang J-K, et al. Iridium-catalyzed highly efficient chemoselective reduction of aldehydes in water using formic acid as the hydrogen source. Green Chem. 2017;19(14):3296–301. https://doi.org/10.1039/c7gc01289f
39. Guo B, Xue J-Y, Li H-X, Tan D-W, Lang J-P. Design of recyclable TEMPO derivatives bearing an ionic liquid moiety and N,N-bidentate group for highly efficient Cu(i)-catalyzed conversion of alcohols into aldehydes and imines. RSC Adv. 2016;6(57):51687–93. https://doi.org/10.1039/c6ra10373a
40. Atta AH, Mouneir SM. Evaluation of some medicinal plant extracts for antidiarrhoeal activity. Phytother Res. 2005;19(6):481–5. https://doi.org/10.1002/ptr.1639 PMID: 16114083
41. Cowan MM. Plant products as antimicrobial agents. Clin Microbiol Rev. 1999;12(4):564–82. https://doi.org/10.1128/CMR.12.4.564 PMID: 10515903
42. Silva N, Fernandes Júnior A. Biological properties of medicinal plants: a review of their antimicrobial activity. J Venom Anim Toxins incl Trop Dis. 2010;16(3):402–13. https://doi.org/10.1590/s1678-91992010000300006
43. Burt S. Essential oils: their antibacterial properties and potential applications in foods--a review. Int J Food Microbiol. 2004;94(3):223–53. https://doi.org/10.1016/j.ijfoodmicro.2004.03.022 PMID: 15246235
44. Balouiri M, Sadiki M, Ibnsouda SK. Methods for in vitro evaluating antimicrobial activity: a review. J Pharm Anal. 2016;6(2):71–9. https://doi.org/10.1016/j.jpha.2015.11.005 PMID: 29403965
45. Nikaido H. Molecular basis of bacterial outer membrane permeability revisited. Microbiol Mol Biol Rev. 2003;67(4):593–656. https://doi.org/10.1128/MMBR.67.4.593-656.2003 PMID: 14665678
46. Borges A, Ferreira C, Saavedra MJ, Simões M. Role of phenolic compounds in antimicrobial activity. Microb Drug Resist. 2013;19(4):256–65.
47. Arif T, Bhosale JD, Kumar N, Mandal TK, Bendre RS, Lavekar GS, et al. Natural products--antifungal agents derived from plants. J Asian Nat Prod Res. 2009;11(7):621–38. https://doi.org/10.1080/10286020902942350 PMID: 20183299
48. Daglia M. Polyphenols as antimicrobial agents. Curr Opin Biotechnol. 2012;23(2):174–81. https://doi.org/10.1016/j.copbio.2011.08.007 PMID: 21925860
49. Othman L, Sleiman A, Abdel-Massih RM. Antimicrobial activity of polyphenols and alkaloids in middle eastern plants. Front Microbiol. 2019;10:911. https://doi.org/10.3389/fmicb.2019.00911 PMID: 31156565
50. Cushnie TPT, Lamb AJ. Antimicrobial activity of flavonoids. Int J Antimicrob Agents. 2005;26(5):343–56. https://doi.org/10.1016/j.ijantimicag.2005.09.002 PMID: 16323269
51. Xie Y, Yang W, Tang F, Chen X, Ren L. Antibacterial activity and mechanism of flavonoids. Crit Rev Food Sci Nutr. 2015;55(1):103–12.
52. Prasad S, Kashyap RS, Deopujari JY, Purohit HJ, Taori GM, Daginawala HF. Effect of Fagonia Arabica (Dhamasa) on in vitro thrombolysis. BMC Complement Altern Med. 2007;7:36. https://doi.org/10.1186/1472-6882-7-36 PMID: 17986325
53. Seelinger G, Merfort I, Schempp CM. Anti-oxidant, anti-inflammatory and anti-allergic activities of luteolin. Planta Med. 2008;74(14):1667–77. https://doi.org/10.1055/s-0028-1088314 PMID: 18937165
54. Doughari JH. Phytochemicals: extraction methods, basic structures and mode of action as potential chemotherapeutic agents. Rijeka, Croatia: INTECH Open Access Publisher; 2012.
55. Ferreira LG, Dos Santos RN, Oliva G, Andricopulo AD. Molecular docking and structure-based drug design strategies. Molecules. 2015;20(7):13384–421. https://doi.org/10.3390/molecules200713384 PMID: 26205061
56. Daina A, Michielin O, Zoete V. SwissADME: a free web tool to evaluate pharmacokinetics, drug-likeness and medicinal chemistry friendliness of small molecules. Sci Rep. 2017;7:42717. https://doi.org/10.1038/srep42717 PMID: 28256516
57. Lipinski CA, Lombardo F, Dominy BW, Feeney PJ. Experimental and computational approaches to estimate solubility and permeability in drug discovery and development settings. Adv Drug Deliv Rev. 2001;46(1–3):3–26. https://doi.org/10.1016/s0169-409x(00)00129-0 PMID: 11259830
58. Varma MVS, Ashokraj Y, Dey CS, Panchagnula R. P-glycoprotein inhibitors and their screening: a perspective from drug discovery. Drug Metab Rev. 2010;42(1):162–93.
59. Testa B, Krämer SD. The Biochemistry of Drug Metabolism. Wiley; 2012.
60. Daina A, Zoete V. A BOILED-Egg to predict gastrointestinal absorption and brain penetration of small molecules. ChemMedChem. 2016;11(11):1117–21. https://doi.org/10.1002/cmdc.201600182 PMID: 27218427